Geophys. J. Int. (2007) **169,** 1180–1200 doi: 10.1111/j.1365-246X.2007.03367.x

Kinematics of the Western Africa-Eurasia plate boundary from focal mechanisms and GPS data

E. Serpelloni,[1] G. Vannucci,[2] S. Pondrelli,[2] A. Argnani,[3] G. Casula,[1] M. Anzidei,[1] P. Baldi[4] and P. Gasperini[4]

[1]*Istituto Nazionale di Geofisica e Vulcanologia – Centro Nazionale Terremoti, Via D. Creti,* 12 – 40128 *Bologna, Italy. E-mail: serpelloni@bo.ingv.it*
[2]*Istituto Nazionale di Geofisica e Vulcanologia, Sezione di Bologna, Bologna, Italy*
[3]*ISMAR—CNR, Geologia Marina, Bologna, Italy*
[4]*Dipartimento di Fisica, Settore di Geofisica, Università di Bologna, Italy*

Accepted 2007 January 25. Received 2007 January 25; in original form 2006 February 1

SUMMARY

The Western Mediterranean displays a complex pattern of crustal deformation distributed along tectonically active belts developed in the framework of slow oblique plate convergence. We used earthquake and Global Positioning System (GPS) data to study the present-day kinematics and tectonics of the Africa-Eurasia plate boundary in this region. Crustal seismicity and focal mechanisms, analysed in terms of seismic moment release and seismic deformation, outline the geometry of major seismic belts and characterize their tectonics and kinematics. Continuous GPS data have been analysed to determine Euler vectors for the Nubian and Eurasian plates and to provide the global frame for a new Mediterranean GPS velocity field, obtained by merging continuous and campaign observations collected in the 1991–2005 time span. GPS velocities and displacements predicted by the Nubia-Eurasia rotation pole provide estimates of the deformation accommodated across the tectonically active belts. The rather simple deformation occurring in the Atlantic region, characterized by extension about perpendicular to the Middle Atlantic and Terceira ridges and right-lateral motion along the Gloria transform fault, turns into a complex pattern of deformation, occurring along broader seismic belts, where continental lithosphere is involved. Our analysis reveals a more complex fragmentation of the plate boundary than previously proposed. The roughly E-W trending mainly compressive segments (i.e. southwestern Iberia, northern Algeria and southern Tyrrhenian), where plate convergence is largely accomodated across rather localized deformation zones, and partially transferred northward to the adjacent domains (i.e. the Algero-Balearic and Tyrrhenian basins), are interrupted by regions of more distributed deformation (i.e. the Rif-Alboran-Betics, Tunisia-Libya and eastern Sicily) or limited seismicity (i.e. the Strait of Sicily), which are characterized by less homogeneous tectonics regimes (mainly transcurrent to extensional). In correspondence of the observed breaks, tectonic structures with different orientation interfere, and we find belts with only limited deformation (i.e. the High and Middle Atlas, the Tunisian Atlas and the offshore Tunisia-Libya belt) that extends from the plate boundary into the Nubian plate, along pre-existing tectonic lineaments. Our analysis suggest that the Sicilian-Pelagian domain is moving independently from Nubia, according to the presence of a right-lateral and extensional decoupling zone corresponding to the Tunisia-Libya and Strait of Sicily deformation zone. Despite the space variability of active tectonic regimes, plate convergence still governs most of the seismotectonic and kinematic setting up to the central Aeolian region. In general, local complexities derive from pre-existing structural features, inherited from the tectonic evolution of the Mediterranean region. On the contrary, along Calabria and the Apennines the contribution of the subducted Ionian oceanic lithosphere and the occurrence of microplates (i.e. Adria) appear to substantially modify both tectonics and kinematics. Finally, GPS data across the Gibraltar Arc and the Tyrrhenian-Calabria domain support the hypothesis that slab rollback in these regions is mostly slowed down or stopped.

Key words crustal deformation, Global Positioning System (GPS), plate boundary, seismicity, seismotectonics,

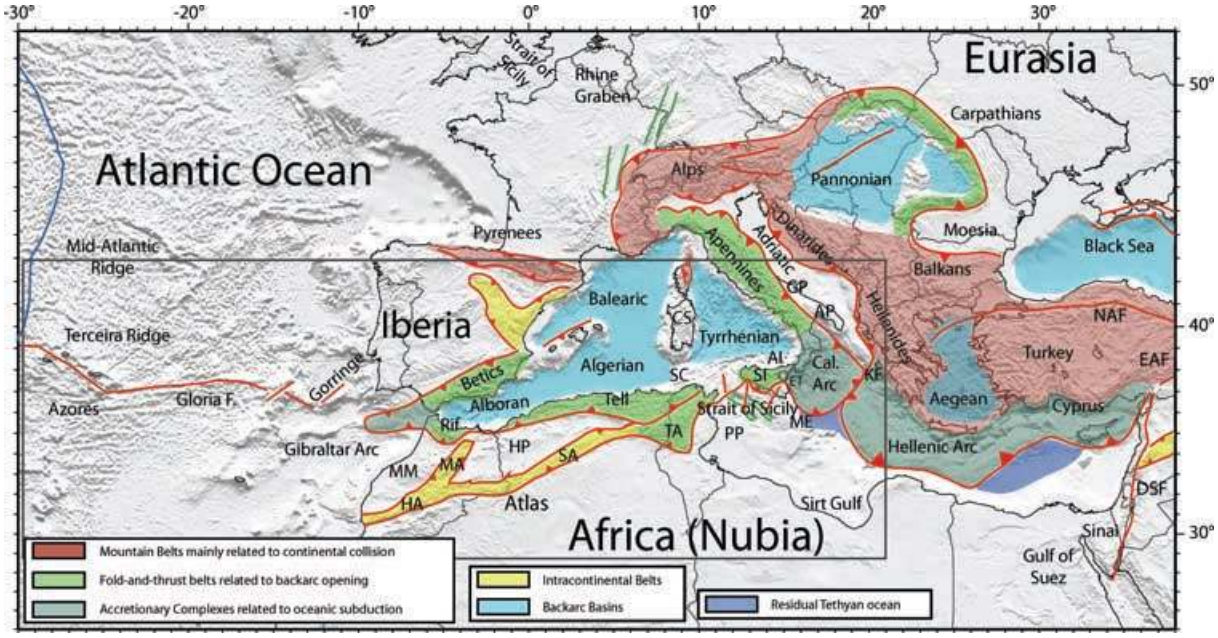

Figure 1. Tectonic sketch of the Mediterranean region. The grey box outlines the area studied in this work (HA: High Atlas; MM: Moroccan Meseta; MA: Middle Atlas; SA: Saharian Atlas; TA: Tunisian Atlas; HP: High Plateau; SC: Sardinia Channel; ME: Malta Escarpment; SI: Sicily; AI: Aeolian Islands; ET: Mount Etna; PP: Pelagian Plateau; CS: Corsica-Sardinia block; AP: Apulian block; GP: Gargano Promontory; KF: Kephallinia Fault zone).

INTRODUCTION

The complex morphology of the Mediterranean region (Fig. 1), characterized by deep basins and arcuate fault-and-thrust belts (FTB), has originated from the long-lasting plate convergence between Africa/Arabia and Eurasia (Dewey *et al*. 1973; Le Pichon *et al*. 1988; Dewey *et al*. 1989), which has been active since the Late Cretaceous, and is currently rather slow (DeMets *et al*. 1994; Calais *et al*. 2003; McClusky *et al*. 2003). The Africa-Eurasia plate boundary displays, from west to east, a transition from simple deformation at the oceanic plate boundaries of the Atlantic, characterized by narrow seismic belts, to a broad belt of seismicity and deformation that characterizes the Alpine belt s.l. (Fig. 2), resulting in a complex pattern of the crustal stress and strain fields (Rebaï *et al*. 1992; Vannucci *et al*. 2004).

Several seismotectonic syntheses have been proposed in the last decades, both at local or regional scale (e.g. Jackson & McKenzie 1988; Ekström & England 1989; Westaway 1990; Rebaï *et al*. 1992; Kiratzi & Papazachos, 1995; Pondrelli *et al*. 1995, Pondrelli 1999). However, the Africa-Eurasia plate boundary is still mostly represented by a simplified compressive lineament from Morocco to Sicily. Nocquet & Calais (2004), using a crude combination of both permanent and non-permanent Global Positioning System (GPS) velocities, proposed a sketch of the Western and Central Mediterranean plate boundary, but did not utilize earthquake data in their analysis. Recently improved catalogues of focal mechanisms

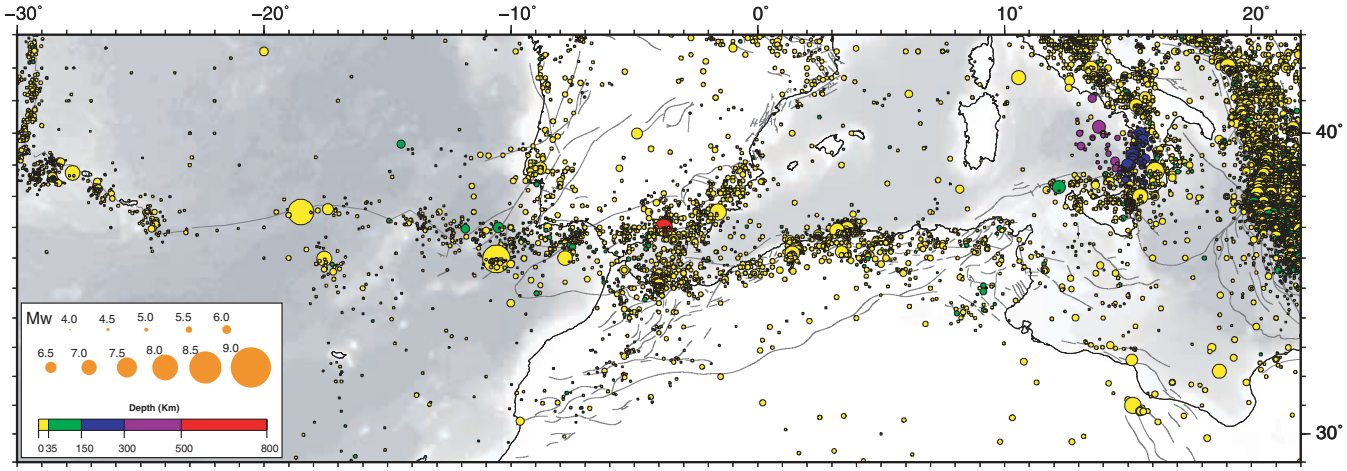

Figure 2. Earthquakes with $M \geq 4$ in the Atlantic and Western Mediterranean region taken from the Karnik (1996) catalogue (data from 1901 to 1964) and International Seismological Centre (ISC) *Bulletin* (data from 1965 to 2004), colour-coded with respect to epicentre depths. Faults, as in the other following figures, are taken from the Geodynamic Map of the Mediterranean compiled in the frame of the Commission for the Geological Map of the World (http://ccgm.free.fr).

(e.g. Vannucci & Gasperini, 2004) allow us to better investigate the pattern of coseismic deformation in terms of active tectonic regimes occurring along the plate boundary zone.

The GPS technique represents a fundamental tool for studying the kinematics of continental deformation at diffuse plate boundaries, allowing us to derive interseismic velocities and velocity gradients. Moreover, due to the great improvement of the global tracking network and GPS infrastructures (i.e. an increasing number of continuously operating stations that allows for a better resolution of the global reference frame), geodetic evaluation of the instantaneous motions of most tectonic plates have become increasingly well constrained. Estimates of present-day Africa-Eurasia Euler vectors have been recently proposed from the analysis of space geodetic data by Sella *et al*. (2002), Calais *et al*. (2003), Fernandes *et al*. (2003), Kreemer *et al*. (2003), McClusky *et al*. (2003), Altamimi *et al*. (2002) and D'Agostino & Selvaggi (2004). The number of GPS stations in the Western Mediterranean, however, cannot exhaustively describe the kinematics of the complex Africa-Eurasia plate boundary system, and an integrated use of GPS data and other independent kinematic indicators (e.g. earthquake focal mechanisms) is, therefore, necessary to provide a better description of the ongoing crustal deformation. Moreover, the analysis of kinematic indicators from different data sources allow us to investigate consistencies and discrepancies among them, strengthening their interpretation.

The aim of this work is to provide a new picture of the present-day kinematics and tectonics of the Western Mediterranean. In order to achieve our goal we use instrumental seismicity, analysed in terms of seismic moment release, to outline the geometry of the major seismically active belts forming the plate boundary. We use the most complete earthquake focal mechanisms catalogue available for the study region to characterize the active tectonic regimes along the plate boundary zone by deriving the orientation of principal strain axes through a seismic moment summation method. We also present a new GPS velocity field at the plate boundary scale, which is obtained by combining GPS surveys, performed during the 1991–2004 time interval, and continuous observations collected in the 1998–2005 time span at stations operating in the Euro-Mediterranean region. GPS velocities are used to frame local and regional tectonic features in the context of the current Africa (Nubia)-Eurasia plate convergence, deriving new absolute and relative Euler rotation poles for the two major plates. We use GPS velocities, together with the predicted Nubia/Eurasia kinematic boundary conditions, to further constrain deformation rates across the major seismic belts, through a series of velocity cross-sections constructed parallel to plate convergence directions.

Despite the limitations and resolution of the data available, mainly due to the short interval of the seismic catalogue compared to the recurrence time for large earthquakes (that might be of several hundreds to thousands years for slowly deforming continental domains) and the still limited number of GPS stations, with respect to the known tectonic complexity of the study region, an integrated use of seismic and geodetic observations of crustal deformation can provide a more comprehensive description of the structural and kinematic complexity of the region, and an improved framework for the analysis of the dynamic processes governing crustal deformation.

WESTERN MEDITERRANEAN TECTONICS

The geology of the Western Mediterranean can be briefly summarized as characterized by a line of looping fold-and-thrust-belts (FTBs) surrounding two main deep-water basins, the Alboran-Algero-Balearic and the Tyrrhenian basins (Fig. 1). To a large extent, the FTBs were originated while the basins were forming in a backarc position (Horvath & Berckhemer, 1982). The Alboran-Algero-Balearic basin extends from the northern coast of Africa to the Gulf of Lions and originated from a Late Oligocene-Aquitanian rifting followed by an Aquitanian–Langhian drifting phase, which led to the emplacement of oceanic crust. The Tyrrhenian basin is located in the wake of the Apennines and Sicilian Meghrebides, and originated by backarc extension from Late Miocene to Pleistocene, with tectonic activity progressively younger towards SE. The amount of extension is greater in the southern part of the basin which is characterized by thin crust (less than 10 km) and high heat flow (Malinverno & Ryan 1986; Patacca *et al*. 1990; Argnani & Savelli 1999).

The NE–SW trending and N-verging Betics Cordillera of Spain and the S-verging Rif of northern Morocco form an arc-shaped mountain belt, mainly deformed during the Miocene (Burdigalian to Tortonian), connected by the Gibraltar Arc (Wildi 1983; Banks & Warburton 1991; Blankenship 1992; Chalouan *et al*. 2001) and continuing to the east into the E-W trending Tell, which follows the northern coast of Africa until Tunisia (Wildi 1983), forming the Maghrebian FTB. In the external Tell deformation continued till the Quaternary by S-SE-propagating thrusts. In Tunisia the Tell merges to the south with the Atlas belt, outlining a broad zone where deformation occurred until the Quaternary. In particular, a large number of small Mesozoic grabens, with trends varying from NW–SE to E–W, have been reactivated in compression during the Quaternary in the southern part of Tunisia (Snoke *et al*. 1988; Anderson 1996).

The Alboran Sea is floored by thinned continental crust (12–20 km thick; Torné *et al.* 2000) and surrounded by the Betics-Rif orocline, where the crust thickens to 25–40 km (Julià & Mejía 2004). The basin opened during the Miocene (Watts *et al*. 1993; Comas *et al*. 1999) and was subsequently affected by strike-slip deformation (Alvarez-Marron 1999). Volcanic activity started in the Early Miocene with calc-alkaline character, to be replaced subsequently by transitional to alkaline products towards the Pliocene. This change in magmatic character is thought to be related to different geodynamic processes including lithospheric root removal (Turner *et al*. 1999), westward slab rollback (Duggen *et al*. 2004), or flows induced by slab tears (Faccenna *et al*. 2004).

The Atlas is an intracontinental high mountain belt originated during the Cenozoic Alpine collision that affected the African craton (Piquet *et al*. 2002; Benaouali-Mabarek *et al.* 2006), and runs almost parallel to the coast of north Africa more than 200 km south of the Rif and Tell. Shortening estimates for the Neogene across the Middle and High Atlas ranges account for 20–40% of Africa-Europe convergence, suggesting that the Atlasic deformation played a major role in the plate boundary evolution (Gomez *et al*. 2000). The blind thrust front that bounds to the south the eastern High Atlas has apparently been reactivated during the Pliocene-Quaternary, particularly toward Tunisia (Vially *et al*. 1994).

The Strait of Sicily interrupts the continuity of the Maghrebian FTB between Northern Africa and Sicily and is characterized by a thinned continental crust (∼20 km thick) and a system of NW–SE trending troughs, deeper than 1000 m, originated mainly during the Pliocene (Argnani 1990). Alkaline volcanic activity has been documented since Tortonian (10–8 Ma) in its western part, and two large volcanic islands (i.e. Pantelleria and Linosa) originated in the last 0.5 Ma. Although a strike-slip origin for the troughs has been proposed (e.g. Boccaletti *et al*. 1987), seismic data indicates that rifting is the most likely tectonic process (Argnani 1990). Oil

industry data have also shown the occurrence of a system of Cretaceous grabens trending from WNW-ESE to NNW-SSE that extends southward from the Pelagian Shelf to the Sirt Gulf and onshore Libya (Jongsma *et al*. 1985). The Libyan grabens mainly originated from a Late Cretaceous-Palaeocene rifting episode. The major boundary faults have been subsequently reactivated, possibly as oblique-slip faults, during the Neogene compressional stress field (van der Meer & Cloetingh 1993).

The Maghrebian FTB of Sicily represents the eastward continuation of the African Tell and is composed of a stack of Meso-Cenozoic sediments deposited along the African passive margin and its adjacent basin and emplaced since the Pliocene (Roure *et al*. 1990). Late Pleistocene sediments seal the thrust front in the southern offshore (Argnani 1987; Patacca & Scandone 2004), although some younger out-of-sequence thrusting has been reported on land (Lickorish *et al*. 1999). Extensional faulting, mainly trending ENE–WSW, affected the northern part of Sicily since Late Messinian, as part of the Tyrrhenian basin opening (Roure *et al*. 1990).

The Calabrian Arc, connects the Maghrebides of Sicily and the Southern Apennines, and is characterized by a stack of basement units older than 260 Ma, coming from different levels of a Hercynian continental crust (e.g. Bonardi *et al*. 2001). A thick Oligocene-Pliocene forearc sedimentary succession crops out on the Ionian side of Calabria, where subduction has been going on till recently, or is still active (Selvaggi & Chiarabba 1995; Chiarabba *et al*. 2005). The external Calabrian Arc (Rossi & Sartori 1981) is a wide accretionary complex that extends into the Ionian Sea to touch the Mediterranean Ridge, SW of Kephallinia, and is confined to the NE and SW by the Apulian and Malta escarpments, respectively (Scandone *et al*. 1981; Biju-Duval *et al*. 1982; Catalano *et al*. 2001). The onshore Calabrian Arc has been affected by major uplift in the last 0.8 Ma, with rates close to 2.0 mm yr^{-1} (Westaway 1993; Bordoni & Valensise 1998), and presents extensional grabens trending NE–SW and NW–SE filled by Late Pliocene-Quaternary sediments (Tortorici *et al*. 1995). The Ionian basin is one of the deeper stretches of the Mediterranean, and its evolution is still open to debate both in term of age of events and nature of its crust. Studies of the crustal velocity structure of the Ionian suggest the presence of an oceanic crust (de Voogd *et al*. 1991). Palaeogeographic reconstructions assign ages that range from Early Cretaceous to Permian for the Ionian oceanic lithosphere (e.g. Dercourt *et al*, 1993; Stampfli *et al*. 1991, 2001; Argnani 2005).

SEISMOLOGICAL DATA AND ANALYSIS

Instrumental seismicity

Fig. 2 shows instrumental seismicity ($M_w \geq 4$) in the 1901–2004 time interval taken from the Karnik Catalogue (Karnik 1996) for earthquakes before 1964, and the International Seismological Centre Catalogue (ISC 2004; http://www.isc.ac.uk) for earthquakes after 1964. Although the ∼100 yr time span of the combined catalogue can not be considered representative of the distribution of largest earthquakes, for which recurrence time might be of several hundreds to thousands years for slowly deforming continental domains, the analysis of the spatial distribution of instrumental seismicity provide indications on how earthquake distribution, and related deformation, is diffuse or localized across the plate boundary.

From the Atlantic ridge to the Central Mediterranean, seismicity is distributed along some known tectonic and morphological features, and entering the Mediterranean outlines a broadly deforming zone. Earthquakes shallower than 35 km in Fig. 2 depict a large-scale image of the Africa-Eurasia plate boundary, marking the boundaries of the main interacting plates, and identifying regions characterized by low or absent seismic release (e.g. Adriatic Sea, Ionian Sea, Central Tyrrhenian Sea and Balearic basin). Events occurring at depths greater than 150 km mark those regions that are related to lithospheric subduction (Fig. 2). In the southernmost part of the Tyrrhenian Sea a clear Wadati-Benioff zone can be recognized by the earthquakes distribution with depth, delineating the northwestward dipping Ionian slab, subducted beneath Calabria and the Tyrrhenian (Chiarabba *et al*. 2005). The other clear deep seismicity in the Mediterranean is present south of the Kephallinia fault zone and delineates the northeastward gently dipping Hellenic subduction plane. Intermediate-depth seismicity (35–150 km) is present beneath the Gibraltar Arc and westernmost Alboran Sea, whereas few deep-focus earthquakes (>500 km) occur beneath southern Spain (Fig. 2). However, some debate still exists regard their attribution to active subduction beneath the Gibraltar Arc (e.g. Calvert *et al*. 2000; Gutscher *et al*. 2002).

In order to better outline the geometry and possible fragmentation of the major plate boundary seismic belt, we use the Karnik and ISC catalogues (including earthquakes with $M_w \leq 4$) to compute the seismic moment release per year and per unit area (i.e. the seismic flux) on a regular $0.5^\circ \times 0.5^\circ$ mesh (Fig. 3). Due to the short time coverage of the earthquake catalogue the seismic flux cannot be considered as representative of the amplitude of active deformation but can only be used as a qualitative tool to outline its spatial distribution. The scalar seismic moment of each earthquake is estimated from the moment magnitude, using the Hanks & Kanamori (1979) relation ($M_0 = 10^{3/2Mw+16.05}$), where the M_w has been previously uniformly determined by using the relations from Gasperini & Ferrari (2000) and Johnston (1996) for the Italian and Mediterranean regions, respectively. For each earthquake we estimate the radius of the seismic crack (i.e. the semi-length of the seismogenic fault derived from the scalar seismic moment of each event) from standard scaling relationships (Kanamori & Anderson 1975) to determine the percentage of the seismic crack area (and then of the scalar seismic moment) falling into each cell of the grid. Then we cumulate the scalar seismic moment for each cell (see the example reported in the lower left inset of Fig. 3) to determine the seismic moment released (in dyne×cm) per unit area (in km^2) and per year, considering the Karnik + ISC time span (i.e. 104 yr) and the area of each cell (Fig. 3). Since in old ISC bulletins the unknown depth of several crustal events is conventionally reported as 33 or 35 km, in our computations we use 35 km as a depth threshold of crustal seismicity at the scale of the plate boundary. Thus, such value is not to be considered as the thickness of the seismogenic layer, in the Kostrov (1974) sense, but only as a conservative limit to avoid the loss of significant crustal earthquakes due to the uncertainty on their depth. In any case, since well-located crustal earthquakes are largely concentrated in the first 10–20 km, we can be confident that our choice is not critical for the aims of this analysis.

Except for 'spots' of large seismic moment release (with values up to $10^{22.5}$ dyne × cm × $km^{-2}yr^{-1}$) related to the largest earthquakes included in the catalogue (e.g. the 1941 central Gloria Fault, the 1969 Gorringe Bank), Fig. 3 outlines some spatially continuous narrower regions (mainly displayed in yellow and orange, and contoured) that provide a clearer picture of the seismically active segments of the Africa-Eurasia plate boundary. The roughly E–W trending seismic belts characterizing the main plate boundary zone

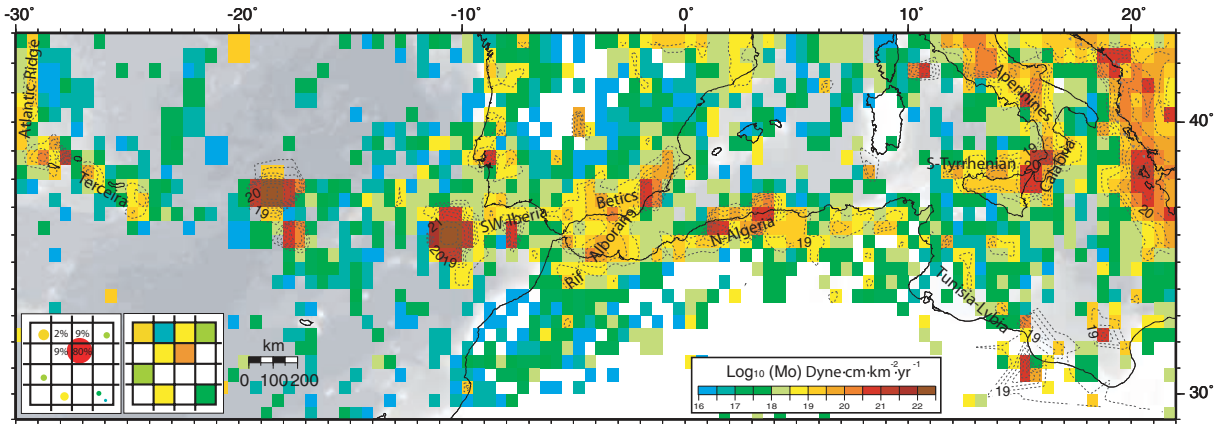

Figure 3. Map of the seismic flux (i.e. the seismic moment released per year and per unit area) computed on a regular 0.5° × 0.5° grid, using all earthquakes with hypocentral depths <35 km. The dashed lines show contouring of larger flux values (>10^{19} dyne × cm × km^{-2} yr^{-1}). The lower left inset displays how the seismic flux is obtained using the seismic crack radius. The percentage of each earthquake area (and the associated scalar seismic moment) is computed and the cumulative scalar seismic moment value is obtained for each cell.

(i.e. Terceira ridge, southwestern Iberia, northern Algeria and southern Tyrrhenian) appear to be interrupted by regions displaying a significantly lower seismic flux (e.g. the western segment of the Gloria Fault and the Strait of Sicily), or by differently oriented belts (e.g. the Rif-Alboran-Betics region and the Tunisia-Libya lineament).

Earthquakes in the Atlantic region are narrowly clustered along the Middle Atlantic ridge, and to the east along the NW–SE trending Terceira ridge, up to the Azores Islands (Figs 2 and 3). Toward the east, the Gloria Fault appears almost seismically silent between longitude 24°W and 19°W, whereas, eastward we observe the high seismic flux localized in correspondence of the great Ms = 8.3, 1941 earthquake. East of the Gorringe Bank (around longitude 12°W), which is dominated by the high seismic flux related to the Ms = 8.0, 1969 earthquake, the area characterized by a higher level of seismic flux (>10^{18} dyne × cm × km^{-2} yr^{-1}) broadens, and entering the Western Mediterranean its distribution becomes more complex, delineating a 'Z-shaped' seismic belt that includes the offshore southwestern Iberia, the Betics, the Alboran and the Rif-Tell belts (Fig. 3). Moving toward the Central Mediterranean, the seismic moment release is lower and the earthquake distribution is sparser (e.g. in the Tunisian shelf), or almost absent (e.g. in the Sardinia Channel and Strait of Sicily). A NW-SE oriented seismic belt runs from northern Tunisia to Libya, with the highest seismic flux values (up to 10^{21} dyne × cm × km^{-2} yr^{-1}) located west of the Sirt Gulf (Fig. 3). In Sicily and Calabria, where moderate to large (M_w > 5.5) magnitude events occur (up to the M = 7.0, 1908 Messina and the M = 7.3, 1905 Calabria earthquakes) the seismic flux shows larger values (up to 10^{20} dyne × cm × km^{-2} yr^{-1}) clustered along an E–W trending belt in northern Sicily and southern Tyrrhenian. Starting from Calabria, the orientation of the major seismic belts changes, following the Apennines range along peninsular Italy (with seismic flux values up to 10^{21} dyne × cm × km^{-2} yr^{-1}) and, on the eastern side of the Adriatic Sea, the NW-SE trending Dinaric-Albanides-Hellenides belts, where the largest seismic cluster of the Mediterranean is present (with seismic flux up to $10^{21.5}$ dyne × cm × km^{-2} yr^{-1} in the Ionian Islands). In the Central Mediterranean, regions characterized by a significantly lower seismic moment release (i.e. the Ionian and southern Adriatic Seas) are surrounded by highly seismic belts (i.e. Apennines and Albanides-Hellenides). The external Calabrian wedge in the Ionian sea, in particular, is characterized by very low seismicity, although this offshore portion of the Calabrian subduction system may be deforming aseismically and, further to the North, locked or partially locked (Gutscher *et al*. 2006).

Earthquake focal mechanisms

In order to study the pattern of seismic deformation along the plate boundary zone we use the largest data set of focal mechanisms available for the study area, which has been obtained merging Moment Tensor (MT) on-line catalogues including: (i) Centroid Moment Tensor (CMT) catalogue by Harvard University (Dziewonski *et al*. 1981, 2000 and references therein); (ii) European Mediterranean Regional CMT catalogue by INGV (Pondrelli *et al*. 2002, 2004a) and (iii) the Eidgenössische Technische Hochschule of Zürich catalogue (Braunmiller *et al*. 2002), as well as from the literature, using the EMMA database by Vannucci and Gasperini (2003, 2004). The EMMA (Version 2.2) database, in particular, consists of a collection of more than 6000 first motion focal solutions, taken from the literature and checked for consistency, applying objective criteria (i.e. correctness of the original solution, authoritativeness of the journal and recentness of the paper) to choose the best solution among duplicates for the same earthquake. In any case, data from MT catalogues, when available, are always preferred with respect to literature. For more details about the EMMA database refer to Vannucci *et al*. (2004) and the web page http://www.ingv.it/seismoglo/atlas.

We derive the seismic strain tensors along the plate boundary zone by summing seismic moment tensors over a 0.5° × 0.5° grid, following well known procedures (e.g. Kostrov 1974; Jackson & McKenzie 1988; Westaway 1992; Pondrelli *et al*. 1995; Vannucci *et al*. 2004). Our choice of analysing focal solutions over a regular grid is made in order to avoid the choice of an arbitrary regionalization of the plate boundary, and to provide the best compromise between resolution and reliability of the derived seismic deformation with the available data. However, where rapid transitions between different regimes are likely to occur, or where a great variability of the tectonic regimes is present, this choice can lead to the sum of non-coherent focal solutions.

Considering that the amplitudes of coseismic strain-rates deduced from the sum of the moment tensors of earthquakes occurred in the

last century (i.e. the time span of our focal mechanisms data set) are likely to be over or underestimated (depending on the occurrence or not of the largest possible shock in such a short time interval), we do not attempt to compute seismic strain rates. Consequently, we limit our analysis to principal strain orientations that, in any case, are reasonably representative of the prevailing deformation regimes of each given cell. This choice is related to difficulties in objectively define the thickness of the seismogenic layer along the plate boundary, a value that greatly affects the strain rates estimates. It is also suggested by the strong uncertainty on the seismic efficiency (i.e. the rate between seismically observable and total strain release) over the area considered in our analysis.

The beach-balls in Fig. 4(a) are representative of the moment tensor sum of all the earthquakes with depth shallower than 35 km within each cell; their size is scaled with the cumulative scalar moment and their location is in the centre of the epicentral distribution, weighted with the earthquakes magnitude (Vannucci *et al*. 2004). The size of the beach-balls is not intended to be a quantitative estimate of the real moment release in each area since the focal mechanism database before 1977 (the starting date of Harvard CMT catalogue) is certainly incomplete due to the sporadic nature of the literature feeding the EMMA database. The tectonic regimes resulting from moment tensor sum are displayed in Fig. 4(b) by a colour representation of the Frohlich (1992, 2001) ternary diagram, where red corresponds to a purely compressive regime, green to strike-slip regimes and blue to purely extensional regimes, while composite colours indicate mixed tectonic regimes (see the inset in Fig. 4(b) for the correspondences). The principal seismic strain directions are shown in Fig. 4(c) as horizontal projections of maximum compression (P) and traction (T) axes of cumulative moment tensor in each cell. Figs 4(b) and (c) outline regions characterized by relatively more uniform tectonic regimes and strain orientation (see the black dashed rectangles in Fig. 4(c)). In order to better display how seismic strain orientation changes along the plate boundary we plot rose diagrams of the P and T axes directions, where, in order to evidence the horizontal component of the strain tensors we weight each axis occurrence as $1 \times \cos$ (axis plunge).

The main features observed in Figs 4(b) and (c) can be correlated with the seismic belts defined in Fig. 3. Along the Middle Atlantic belt an extensional regime prevails, whereas along the E–W trending Terceira ridge, strike-slip and extensional regimes coexist. Strike-slip regimes, although sparse, characterize the active deformation up to the Gorringe Bank, whereas compressive regimes prevail along the southwestern Iberia seismic belt. Entering the Mediterranean, mainly strike-slip to extensional tectonic regimes characterize the Betics-Alboran-Rif seismic belts. Whereas compressional and, secondary strike-slip, regimes are present along the northern Algeria seismic belt, with sparser compression occurring in the Algero-Balearic basin. While in Tunisia different tectonic regimes coexist, a strongly coherent strike-slip regime characterizes the Tunisia-Libya NW-SE trending seismic belt. The southern-Tyrrhenian seismic belt displays a clear compressive tectonic regime, whereas eastern Sicily is characterized by strike-slip to extensional regimes. Along the Calabria-Apennines seismic belt extensional regimes prevails.

GPS DATA ANALYSIS AND NUBIA-EURASIA CONVERGENCE

We process GPS observations collected at more than 80 non-permanent geodetic stations during repeated campaigns performed from 1991 to 2004 on regional, subregional and local networks (more details in Serpelloni *et al*. 2002; Serpelloni *et al*. 2005). In this work we use additional data from the 2003 reoccupation of the Aeolian Islands and Pantelleria geodetic points. We process continuous GPS (CGPS) observations collected in the 1998–2005 time span at stations belonging to several networks operating in the Euro-Mediterranean region. In particular, we analyse data coming from the International GPS Service for Geodynamics (IGS), European Permanent GPS Network (EPN-EUREF) and Agenzia Spaziale Italiana (ASI) networks, with additional observations from the Istituto Nazionale di Geofisica e Vulcanologia (INGV) network, for the Italian area. We also analyse data from some stations in Morocco and Egypt, installed by the Massachusetts Institute of Technology Geodesy and Geodynamics group and available through the UNAVCO (http://www.unavco.org) archive. We analyse the whole data set in a three-step approach (Dong *et al*. 1998), following a distributed session strategy (Blewitt *et al*. 1993), by means of the GAMIT/GLOBK and QOCA software (Dong *et al*. 2002; Herring 2004; King & Bock 2004).

In the first step, we use daily GPS phase observations to estimate station coordinates, atmospheric zenith delay, orbital and Earth orientation parameters by means of the GAMIT software, applying loose constraints to geodetic parameters. In each daily processing we use a set of common stations for all the subnetworks analysed, including a number of stations that observed almost continuously from 1991 to 2005. The common sites are used successively to tie together each independent solution, allowing for a uniform reference frame definition.

In the second step we use the GLOBK software to combine, on a daily basis, our loosely constrained solutions with global (IGS1, IGS2, IGS3, IGS4 and IGS5) and regional (EURA and EMED) loosely constrained solutions provided by SOPAC (http://sopac.ucsd.edu). In this step both orbital and common station parameters are estimated and removed for forward analysis, and only loose constraints are applied.

In the third step we define the reference frame for our velocity solution applying generalized constraints (Dong *et al*. 1998; 2002) while estimating a seven-parameter Helmert transformation. In this step we obtain station position time-series that are later used to fit constant velocities and additional parameters (i.e. jumps and seasonal terms). Specifically, we define the reference frame by minimizing the horizontal velocities of 50 IGS core stations with respect to the IGS00 realization of ITRF2000-NNR frame (Altamimi *et al*. 2002; Ray *et al*. 2004). The network parameters are computed separately for each individual daily solution, taken as independent from one another, thus preserving the consistency in the reference frame definition for the entire observation time span. We derive station velocities using the L-1 norm-based robust-fit algorithm embedded in the QOCA software. In this step, annual and semi-annual seasonal signals and offsets due to changes in the CGPS station configuration, as obtained from the station log-files, are computed and removed from the time-series.

Realistic station velocity errors are computed adopting the approach of Mao *et al*. (1999) and Dixon *et al*. (2000), who developed an empirical model for estimating the GPS rate errors for individual velocity components using position time-series in presence of combined white and coloured noise (i.e. flicker and random-walk). For each station, and for each position component, we compute white and coloured noise amplitudes using the weighted root mean squares obtained from the analysis of each position component and the linear relationship given by Dixon *et al*. (2000), to compute noise values for each noise component. It is worth noting that this choice could turn out in over conservative uncertainties (Mao *et al*. 1999).

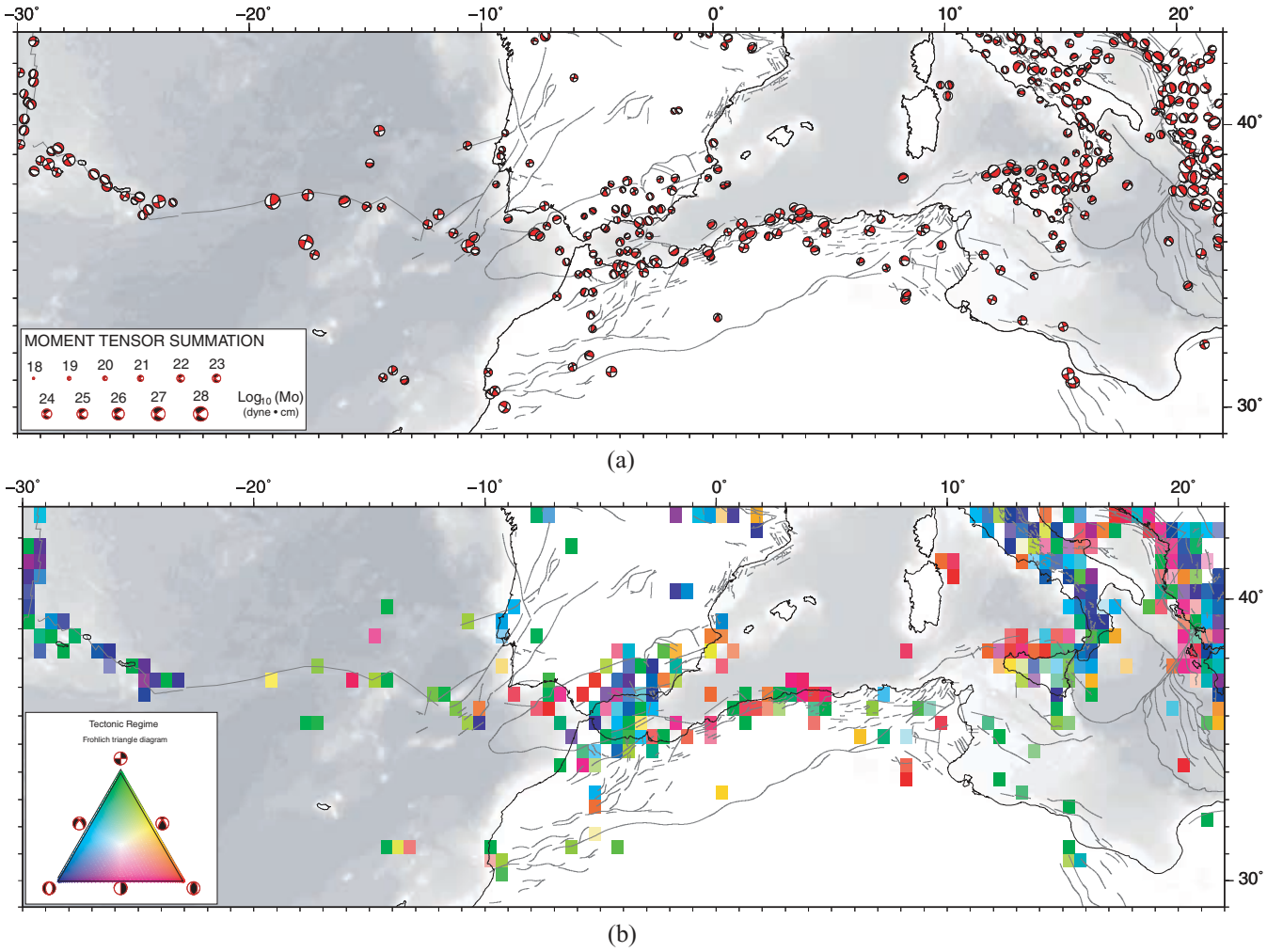

Figure 4. (**a**) Cumulative moment tensors computed using the Kostrov (1974) seismic moment summation method on a regular 0.5° × 0.5° grid. The EMMA (version 2) and MT data sets (with hypocentral depths <35 km) have been used in the computation. For more details on the data sets used see Vannucci *et al*. (2004) and the web page: http://www.ingv.it/seismoglo/atlas. The beach balls are plotted in the barycentre of the epicentral distribution, weighted by the earthquake magnitude, within each cell. (**b**) Tectonic regimes obtained from the sum of moment tensors (Fig. 4a) applying the Frohlich ternary diagram methodology (Frohlich 1992, 2001). (**c**) Horizontal projections of P (in red) and T (in blue) deformation axes, derived from the sum of moment tensors (Fig. 4a), plotted at the centre of each cell. Grey arrows show the displacement vectors of Nubia with respect to Eurasia as predicted by the Euler poles computed in this work (see Fig. 5). The dashed rectangles delineate domains characterized by relatively uniform tectonic regimes (as derived from Fig. 4b) and strain axes orientation. The rose diagrams show for each domain the main P and T axes directions with a 6° sampling interval. In order to evidence the horizontal component of the strain tensors, we weight each axis occurrence as 1 × cos (axis plunge). Black open arrows show the predicted Nubia-Eurasia plate convergence directions. The green open arrow shows the displacement direction of Sicily with respect to Eurasia.

Velocities and one standard deviation uncertainties are listed in Table 1.

We use horizontal velocities and uncertainties of CGPS stations located on tectonically stable domains of the Eurasian and Nubian plates to derive absolute and relative Euler rotation vectors for the two plates. We first select sites thought to be representative of stable plate interiors, and then we use an iterative least-square method, based on a reduced chi-square statistics, to search for the best-fit rotation poles.

The Eurasian Euler pole is estimated using 25 CGPS stations, located in central and eastern Europe, Russia, Artic Islands and eastern Eurasia, and provides a good fit (east and north weighted velocity residuals of 0.46 and 0.38 mm yr^{-1}). The Nubian Euler pole is estimated using nine stations, providing a good fit at GPS stations widely distributed around the plate (East and North weighted velocity residuals of 0.55 and 0.49 mm yr^{-1}). Table 1a shows residual velocities (observed minus calculated) of stations used to define the plate models, while the computed Euler vectors, with one standard deviation uncertainties, are given in Table 2. Our Nubia-Eurasia relative rotation vector provides a good fit to CGPS data well distributed around the two plates, confirming that both are internally rigid at a submm yr^{-1} level on a plate-wide basis (Calais *et al*. 2003; McClusky *et al*. 2003), although more local deformation that does not affect the overall plate coherence cannot be ruled out at the scale of this study. Fig. 5 displays the Africa-Eurasia kinematic boundary conditions, along a simplified plate boundary, predicted by our rotation pole (red arrows), compared with predictions by the NUVEL-1A (DeMets *et al*. 1994) and Calais *et al*. (2003) geological models, and predictions by some previous geodetically determined rotation vectors (see Fig. 5 for more details).

Discrepancies between the Africa-Eurasia convergence predicted by geological (e.g. Nuvel-1A, DeMets *et al*. 1994; Calais *et al*. 2003)

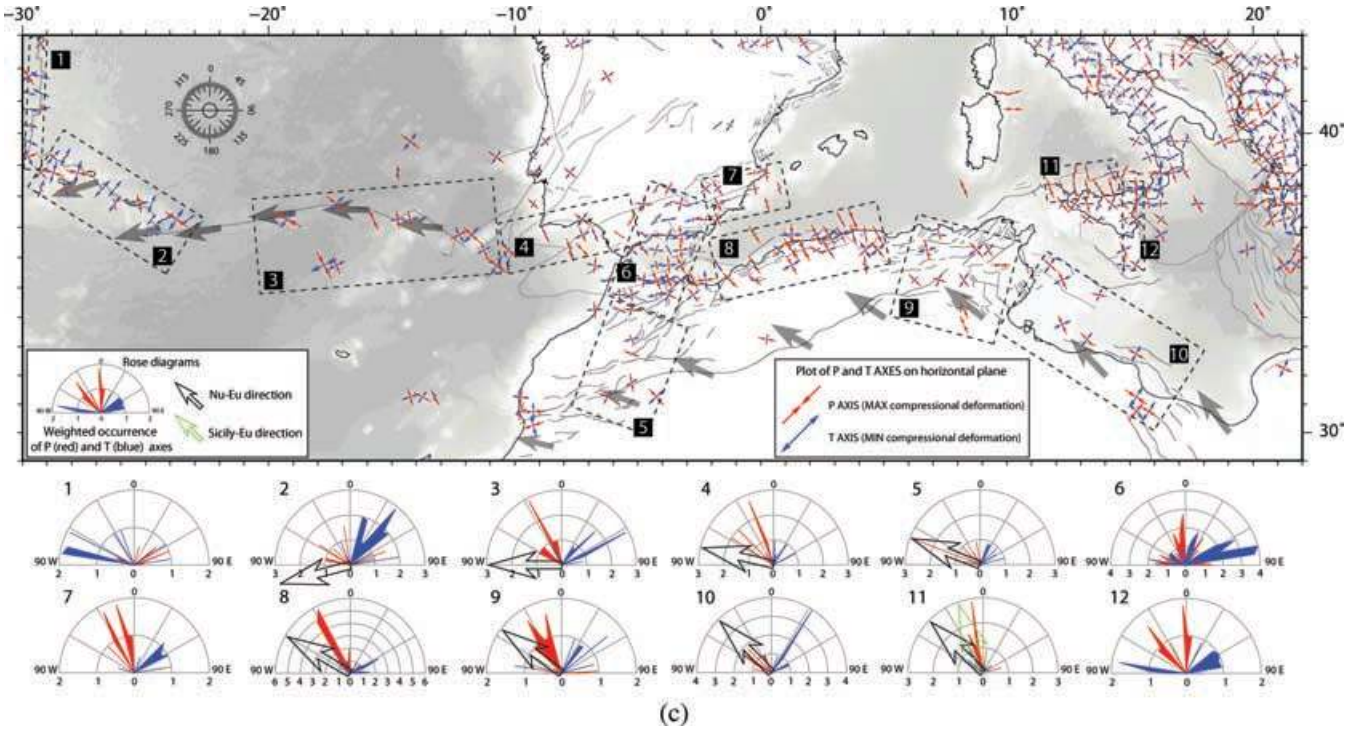

Figure 4. (*Continued*.)

and geodetically derived plate models (Fig. 5) are a well known feature (e.g. Sella *et al*., 2002; Calais *et al*., 2003; McClusky *et al*., 2003). Calais *et al*., (2003) interpreted these observations as possible changes in last 3 Ma Africa-Eurasia relative motion, related to effect of the ongoing continent-continent collision. Despite different locations of the geodetically derived relative Euler poles (see Fig. 5 inset), differences among predicted plate convergence rate and orientation are rather small in the Western Mediterranean (of the order of the 1 mm yr^{-1} level). Differences may be due to the different data sets used, also considering that the Nubian plate is still less constrained by GPS stations than the Eurasian plate. Fig. 5 clearly shows that from convergence in the central Mediterranean, deformation progressively changes westward to transpression (Algeria-Morocco), strike-slip (Gloria fault), and transtension (Azores).

Our velocity solution shares several stations with the Eastern Mediterranean velocity field published in McClusky *et al*. (2000) (see Table. 1), allowing for a rigorous integration of the two velocity fields. We align the McClusky *et al*. (2000) velocities to our stable Eurasia frame of reference applying a seven-parameter Helmert transformation, obtained by finding the transformation that minimize the rms of differences between velocities of common sites. The average discrepancies are small, and the rms for the 24 common stations is 0.8 mm yr^{-1}. Figs 6(a) and (b) display the combined velocity field with respect to stable Eurasia, with 95% confidence ellipses.

Fig. 7 shows residual velocities (only for some plate boundary stations) with respect to our Nubian plate. It is worth noting that in our least squares inversion we do not include the velocities from McClusky *et al*. (2000) stations in Egypt (i.e. HELW, MEST and MATR), but their very small residuals (<0.8 mm yr^{-1}) with respect to our Nubian fixed frame (Fig. 7) confirm the reliability and robustness of our reference frame definition. While the kinematics of the Somalia plate is not well determined by our data, Fig. 7 shows that the Sinai block is moving N-ward with respect to Nubia at a level of $\sim$3 mm yr^{-1}, in agreement with Wdowinski *et al*. (2004).

PRESENT-DAY DEFORMATION ACROSS THE AFRICA-EURASIA PLATE BOUNDARY

The analysis of crustal seismicity provides a picture of the major seismically active belts (Fig. 3) and allows us to characterize the tectonic regimes acting along the plate boundary (Figs 4a–c), while GPS data provide constraints about the kinematics and deformation accomodated across it. Moreover, GPS data allow us to define the active tectonic regimes of regions where few focal solutions are available (i.e. Moroccan Atlas) or where most of deformation is likely to occur aseismically (e.g. Strait of Sicily).

The relatively low number and non-homogeneous distribution of GPS stations in the study region prevent any reliable computation of a long-wavelength velocity gradient field at this scale. However, the velocities predicted by the Nubia-Eurasia rotation pole at points located south of the Atlas mountain range, where no significant deformation is expected to occur (Figs 3, Figs 4a and b), together with the observed GPS velocities can provide values of the deformation rates accommodated within the tectonically active belts. Quantitative estimates of geodetic deformation are obtained by projecting the horizontal GPS velocities along several profiles (Figs 8 and 9), constructed along the direction of Nubia-Eurasia convergence or perpendicularly to the tectonic structures.

In this section we summarize the main tectonic and kinematic features observed along the seismically active belts outlined in Figs 3, 4(a)–(c), and propose a summary sketch of the kinematics and active tectonics as evidenced by our data sets (Fig. 10).

Table 1. GPS velocities and uncertainties (in mm yr^{-1}). From left to right: four characters site code; Longitude; Latitude; ITRF00 velocities; 1σ uncertainties; residual velocities with respect to Eurasia; absolute motion rate and uncertainty. Stations marked with an asterisk are in common with the McClusky *et al*. (2000) velocity solution. Other common stations not reported in the table or the figures are: NSSP, ZECK, KATZ, TELA, POL2, KIT3, METS, TROM and ONSA. See the text for more details.

			Velocity (mm yr^{-1})		Uncertainty (mm yr^{-1})		Residual velocity (mm yr^{-1})		Motion rate (mm yr^{-1})	
Site ID	Lon.	Lat.	East	North	East	North	East	North	Value	1σ
Eurasian plate										
ARTU	58.56	56.43	25.26	4.89	0.44	0.44	−0.02	0.41	0.41	0.44
BOGO	21.04	52.48	21.49	14.03	0.33	0.38	0.37	0.83	0.91	0.39
BOR1*	17.07	52.28	20.76	13.97	0.38	0.39	0.34	0.12	0.36	0.38
BRUS*	4.36	50.80	17.78	15.19	0.38	0.39	−0.41	−0.28	0.50	0.38
GLSV	30.50	50.36	22.55	11.75	0.39	0.39	−0.53	0.34	0.63	0.39
HERS*	0.34	50.87	17.38	15.26	0.39	0.40	0.06	−0.57	0.57	0.40
IRKT	104.32	52.22	24.11	−8.52	0.38	0.39	−0.54	−0.29	0.62	0.38
JOZE*	21.03	52.10	21.52	13.35	0.38	0.39	0.33	0.14	0.36	0.38
KOSG*	5.81	52.18	18.90	15.65	0.39	0.40	0.73	0.32	0.80	0.39
KSTU	92.80	55.98	24.45	−5.37	0.39	0.40	−0.71	−0.16	0.73	0.39
LAMA	20.67	53.89	20.41	13.48	0.38	0.39	−0.35	0.21	0.41	0.38
MDVO	37.22	56.03	23.95	9.85	0.46	0.47	0.85	−0.09	0.86	0.46
MOPI	17.27	48.37	21.10	14.05	0.44	0.47	−0.11	0.22	0.25	0.46
NRIL	88.37	69.35	21.98	−3.31	0.50	0.51	−0.67	0.68	0.95	0.50
NVSK	84.00	54.88	25.93	−3.02	0.52	0.54	0.09	−0.26	0.27	0.53
NYA1*	11.87	78.93	11.48	14.37	0.39	0.39	−0.19	−0.22	0.29	0.39
POLV	34.54	49.60	23.22	11.00	0.59	0.64	−0.57	0.46	0.73	0.58
POTS*	13.07	52.38	19.70	14.16	0.39	0.39	0.09	−0.28	0.29	0.39
PTBB	10.46	52.30	19.56	15.35	0.47	0.51	0.45	0.56	0.72	0.50
TIXI	128.87	71.63	16.22	−13.09	0.41	0.41	0.26	0.31	0.41	0.41
UZHL	22.30	48.63	21.52	12.98	0.46	0.47	−0.52	−0.01	0.52	0.46
WROC	17.06	51.11	20.21	13.21	0.33	0.32	−0.44	−0.65	0.78	0.32
WSRT	6.60	52.92	18.18	15.55	0.39	0.39	0.02	0.31	0.31	0.39
WTZR*	12.88	49.14	20.87	14.54	0.39	0.40	0.62	0.07	0.62	0.38
ZWEN*	36.76	55.70	23.71	10.27	0.39	0.40	0.62	0.23	0.66	0.38
Nubian plate										
GOUG	−9.87	−40.15	20.39	18.12	0.40	0.41	0.02	0.93	0.93	0.41
HARB	27.71	−25.89	16.15	17.07	0.51	0.53	−0.85	−0.13	0.86	0.51
HRAO	27.69	−25.89	17.01	17.22	0.39	0.39	0.01	0.02	0.02	0.39
MAS1	−15.63	27.76	16.12	16.16	0.39	0.40	0.40	−0.36	0.54	0.39
NKLG	9.67	0.35	20.75	18.01	0.47	0.48	−0.96	−0.17	0.97	0.47
PHLW*	31.34	29.86	22.61	17.36	0.65	0.68	0.34	0.57	0.66	0.67
SUTH	20.81	−32.38	16.90	18.01	0.39	0.40	0.54	0.24	0.59	0.39
TGCV	−22.98	16.76	18.25	15.13	0.93	0.79	0.21	−0.30	0.37	0.77
YKRO	−5.24	6.87	21.20	16.83	0.44	0.45	0.18	−0.80	0.82	0.45

Atlantic Region, Terceira Ridge, Gloria Fault and Gibraltar

Seismicity is concentrated in a narrow belt along the roughly N–S trending Middle Atlantic ridge. Earthquakes have generally moderate magnitude (<5.5) and focal mechanisms outline a rather simple pattern, with E–W to ESE–WNW (i.e. ridge normal) oriented extension (Fig. 4c). A ridge-ridge-transform triple junction occurs near the Azores Islands, where the Middle Atlantic ridge meets the NW–SE trending Terceira ridge and where both extensional and strike-slip regimes are present (Fig. 4b). The prevailing NE-SW oriented extension is partly responsible for volcanism of the Azores, and strike-slip events, accordingly to the relative Nubia-Eurasia motion, indicate a right-lateral component of motion (Fig. 4c). Deformation along the Terceira ridge appears rather localized along a relatively narrow band (Fig. 3), following the islands alignment and the neighbouring submarine ridges, on agreement with the pattern of crustal deformation derived from the analysis of local GPS data (Fernandes *et al*. 2006).

Toward the east, the plate boundary evolves into a right-lateral transform fault (i.e. the Gloria Fault), which separates the Eurasian and Nubian plates (Searle 1980; Madeira & Ribeiro 1990) and connects the simple extensional regime of the mid-ocean ridge to the more complex tectonics of the Gibraltar region, characterized by thrust faults and NE–SW trending push-up structures, also involving oceanic lithosphere (Hayward *et al*. 1999; Zitellini *et al*. 2004). The Gloria Fault along its central segment displays a region of scarce seismicity, although an isolated event, the 1941 $M_s = 8.3$, contributes to almost the whole seismic moment release of the region for the last hundred years (Fig. 3). Focal mechanisms indicate a tectonic regime that is mainly strike-slip to transpressive, with *P*-axes oriented N30°W (Fig. 4c). The kinematic boundary conditions given by our Nubia-Eurasia rotation pole (Fig. 5) confirm a right-lateral motion, at a rate of ∼4.7 mm yr^{-1}, along the Gloria Fault between the Terceira Ridge and the Gorringe Bank.

Approaching the Gibraltar Strait (east of longitude 14°W), and entering into transitional to continental domains,

Table 1. (*Continued*.)

Site ID	Lon.	Lat.	Velocity (mm yr^{-1}) East	Velocity (mm yr^{-1}) North	Uncertainty (mm yr^{-1}) East	Uncertainty (mm yr^{-1}) North	Residual velocity (mm yr^{-1}) East	Residual velocity (mm yr^{-1}) North	Motion rate (mm yr^{-1}) Value	Motion rate (mm yr^{-1}) 1σ
Other permanent GPS stations										
AJAC	8.76	41.93	21.1	14.8	0.5	0.5	0.3	−0.2	0.4	0.5
ALAC	−0.48	38.34	20.2	15.4	0.4	0.5	0.3	−0.5	0.6	0.5
ALME	−2.46	36.85	18.8	14.3	0.4	0.5	−0.9	−1.8	1.9	0.5
ANKR*	32.76	39.89	0.6	10.8	0.5	0.6	−24.1	−0.2	24.1	0.5
AQUI	13.35	42.37	21.3	16.0	0.4	0.5	−0.2	1.5	1.6	0.5
BELL	1.40	41.60	19.8	15.0	0.4	0.5	0.2	−0.7	0.8	0.5
BRAS	11.11	44.12	21.6	15.9	0.5	0.5	0.7	1.2	1.4	0.5
BRIX	10.23	45.55	20.7	15.3	0.7	0.8	0.2	0.4	0.5	0.8
BSHM	35.02	32.78	21.4	19.2	0.4	0.4	−3.8	8.7	9.5	0.4
BUCU	26.13	44.46	23.2	11.3	0.4	0.4	−0.1	−1.0	1.0	0.4
CACE	−6.34	39.48	18.8	15.5	0.6	0.5	0.2	−0.8	0.8	0.5
CADM	16.27	41.08	23.9	18.1	0.6	0.6	1.6	4.1	4.4	0.6
CAGL	8.97	39.14	21.8	15.1	0.4	0.4	0.5	0.1	0.5	0.4
CAME	13.12	43.11	22.6	16.9	0.5	0.5	1.2	2.4	2.7	0.5
CANT	−3.80	43.47	19.1	15.3	0.7	0.8	0.9	−0.8	1.2	0.7
CASC	−9.42	38.69	17.3	16.0	0.6	0.5	−0.9	−0.4	1.0	0.6
COSE	16.31	39.20	25.0	16.2	0.5	0.5	2.6	2.2	3.4	0.5
CRAO	33.99	44.41	24.3	11.8	0.9	0.7	−0.1	1.1	1.1	0.7
DUBR	18.11	42.65	22.6	16.6	0.5	0.5	0.3	2.9	2.9	0.5
ELBA	10.21	42.75	20.8	15.1	0.5	0.5	−0.1	0.3	0.3	0.5
GENO	8.92	44.42	21.1	14.7	0.4	0.4	0.7	−0.3	0.8	0.4
GRAS	6.92	43.76	21.1	15.1	0.4	0.4	0.9	−0.1	0.9	0.4
GRAZ*	15.49	47.07	22.5	14.4	0.4	0.4	1.4	0.3	1.4	0.4
IFRN	−5.11	33.54	16.9	16.3	0.5	0.5	−3.0	0.1	3.0	0.5
INGR	12.52	41.83	21.9	16.2	0.5	0.5	0.4	1.6	1.7	0.5
ISTA	29.02	41.10	25.6	9.4	0.5	0.5	1.6	−2.3	2.8	0.5
LAGO	−8.67	37.10	16.9	15.8	0.6	0.8	−1.7	−0.6	1.8	0.6
LAMP	12.61	35.50	20.1	17.5	0.4	0.4	−2.2	2.9	3.7	0.4
LAUG	35.67	34.12	21.8	21.5	0.7	0.8	−3.5	11.1	11.7	0.8
MAD2	−4.25	40.43	18.7	14.8	0.6	0.6	0.0	−1.4	1.4	0.6
MATE	16.70	40.65	23.6	18.3	0.4	0.4	1.3	4.3	4.5	0.4
MEDI	11.65	44.52	23.4	16.8	0.4	0.4	2.5	2.1	3.3	0.4
MILO	12.60	38.00	20.5	17.7	0.6	0.6	−1.6	3.1	3.5	0.6
NICO*	33.40	35.14	18.9	14.3	0.4	0.4	−6.1	3.5	7.0	0.4
NOT1	14.99	36.88	20.9	18.8	0.5	0.5	−1.6	4.6	4.9	0.5
ORID	20.79	41.13	24.0	10.8	0.5	0.5	1.1	−2.4	2.7	0.5
PDEL	−25.66	37.75	12.3	14.1	0.6	0.7	−3.2	−2.2	3.9	0.6
PRAT	11.10	43.89	21.7	16.1	0.5	0.5	0.8	1.4	1.6	0.5
RABT	−6.85	34.00	16.5	16.4	0.5	0.5	−3.0	0.1	3.0	0.5
RAMO	34.76	30.60	22.5	19.1	0.4	0.4	−2.8	8.6	9.0	0.4
SFER	−6.21	36.46	16.7	16.2	0.4	0.4	−2.5	0.0	2.5	0.4
SOFI	23.40	42.56	23.7	11.4	0.6	0.6	0.6	−1.4	1.5	0.6
SRJV	18.41	43.87	23.3	14.8	0.5	0.6	1.1	1.2	1.6	0.5
TETN	−5.36	35.56	16.1	16.0	0.5	0.6	−3.4	−0.2	3.4	0.5
TOUL	1.48	43.56	20.2	15.6	0.6	0.6	1.0	−0.1	1.0	0.6
TGRC	15.65	38.11	24.1	16.6	0.5	0.5	1.6	2.5	3.0	0.5
TITO	15.72	40.60	22.3	18.2	0.5	0.5	0.1	4.1	4.1	0.5
TUBI	29.45	40.79	22.2	9.6	0.7	0.7	−1.9	−2.1	2.8	0.7
UNPG	12.36	43.12	21.9	15.8	0.4	0.4	0.6	1.3	1.4	0.4
VILL	−3.95	40.44	20.1	15.5	0.4	0.4	1.2	−0.6	1.4	0.4
VLUC	15.27	40.23	22.1	16.2	0.4	0.4	0.0	2.0	2.0	0.4
VVLO	13.62	41.87	22.4	16.8	0.5	0.5	0.7	2.5	2.6	0.5
ZIMM*	7.47	46.88	20.2	15.1	0.4	0.4	0.5	−0.1	0.5	0.4

deformation becomes more distributed (Figs 2 and 3). While a dominantly strike-slip regime is observed up to the Gorringe bank (around longitude 10°W), compression becomes dominant eastward and continues along a belt that extends from offshore south Portugal to south Spain, and that partially corresponds to the northern segment of the Gibraltar Arc. Along this WSW-ENE trending seismic belt *P*-axes are oriented N25°W to N45°W (Fig. 4c). GPS data and Nubia-Eurasia predicted displacement rates (profiles 1^{p} and 2 in Figs 8 and 9) show that this belt accommodates between 1.4 and 1.7 ± 0.5 mm yr^{-1} of NW–SE oriented shortening, according to the observed tectonic regime.

Table 1. (*Continued*.)

			Velocity (mm yr^{-1})		Uncertainty (mm yr^{-1})		Residual velocity (mm yr^{-1})		Motion rate (mm yr^{-1})	
Site ID	Lon.	Lat.	East	North	East	North	East	North	Value	1σ
Non−permanent GPS stations										
ALCD	14.36	38.53	19.90	18.07	0.76	0.71	−2.33	3.79	4.45	0.73
ALGE	3.11	36.74	20.01	16.51	0.82	0.82	−0.68	0.90	1.12	0.82
ANGE	15.95	41.71	23.77	18.50	0.54	0.58	1.71	4.46	4.78	0.58
ARZE	−0.31	35.86	18.98	17.30	0.81	0.83	−1.29	1.40	1.90	0.82
CAPR	14.22	40.55	19.63	17.15	0.55	0.56	−2.31	2.85	3.67	0.56
CASS	13.94	41.54	19.90	15.46	0.60	0.60	−1.86	1.12	2.17	0.60
CAST	12.06	43.13	19.60	16.05	0.62	0.65	−1.59	1.46	2.16	0.63
CATA	16.60	38.93	25.12	14.76	0.52	0.53	2.59	0.82	2.72	0.52
CIRP	15.02	40.86	22.12	16.32	0.67	0.71	0.09	2.14	2.14	0.71
CPRN	12.93	41.88	20.53	17.24	0.75	0.75	−1.01	2.76	2.94	0.75
FILI	14.58	38.56	23.32	18.28	0.68	0.69	1.06	4.03	4.17	0.69
IGOU	20.25	39.53	15.38	13.16	0.78	0.78	−7.63	−0.19	7.63	0.78
INGR	12.52	41.83	21.57	16.24	0.58	0.58	0.09	1.71	1.71	0.58
KARI	20.67	39.73	19.52	16.68	1.25	1.41	−3.52	3.40	4.89	1.33
KAST	21.14	37.89	9.27	−5.48	0.77	0.81	−14.04	−18.68	23.37	0.79
LAMO	12.57	35.52	20.53	17.59	0.62	0.63	−1.78	3.06	3.54	0.62
LEFK	20.69	38.85	21.04	1.59	0.76	0.79	−2.10	−11.69	11.88	0.79
MIL0	12.58	38.00	20.97	17.23	0.65	0.68	−1.05	2.70	2.90	0.67
MIRA	14.27	41.64	23.29	17.73	0.73	0.78	1.49	3.44	3.75	0.77
MODE	10.95	44.63	22.06	17.03	0.57	0.58	1.32	2.29	2.64	0.58
MSIC	13.46	43.55	22.73	16.87	0.52	0.53	1.36	2.47	2.82	0.53
PACE	15.52	38.27	22.59	18.21	0.49	0.50	0.15	4.10	4.11	0.50
PANA	15.07	38.63	21.67	16.27	0.64	0.71	−0.66	2.10	2.20	0.70
PANT	11.95	36.83	21.34	15.91	0.47	0.50	−0.73	1.30	1.49	0.49
PIED	14.37	41.37	24.13	14.49	0.77	0.81	2.28	0.22	2.29	0.77
PONZ	12.95	40.91	21.87	16.37	0.58	0.58	0.18	1.90	1.91	0.58
PORO	15.91	38.60	25.02	18.44	0.48	0.54	2.56	4.39	5.08	0.53
SALI	14.87	38.56	23.12	15.78	0.73	0.84	0.81	1.58	1.78	0.82
SGIO	14.66	40.78	22.55	15.98	0.76	0.86	0.57	1.75	1.84	0.85
SPEC*	18.46	40.06	23.66	17.41	0.52	0.54	0.99	3.76	3.89	0.53
SPER	13.46	41.26	20.40	16.22	0.77	0.72	−1.32	1.82	2.25	0.74
STRO	15.24	38.80	22.66	16.12	0.59	0.65	0.33	1.97	2.00	0.64
TREM	15.51	42.12	23.85	18.11	0.57	0.58	1.92	4.00	4.44	0.58
USTI	13.15	38.70	21.50	16.64	0.64	0.58	−0.52	2.19	2.25	0.59
VULC	14.99	38.38	21.75	22.79	0.58	0.59	−0.60	8.60	8.62	0.59

Table 2. Absolute and relative Euler rotation vectors for the Eurasian and Nubian plates. From left to right: Plate name; Longitude; Latitude; 1σ uncertainty in Longitude; 1σ uncertainty in Latitude; rotation rate, 1σ uncertainty of rotation rate; number of stations used to compute the Euler vectors; normalized root mean squares of the inversion; weighted root means squares of velocity residuals for the East and North components (in mm yr^{-1}), respectively

Plate	Lon. (°E)	Lat.(°N)	σ (Lon)	σ (Lat)	ω (° Myr^{-1})	$\sigma(\omega)$	N. sites	χ_v^2	wrms (East)	wrms (North)
Eurasia	−105.66	52.92	0.46	1.11	0.246	0.001	25	1.057	0.460	0.385
Nubia	−81.07	50.05	0.96	1.12	0.254	0.002	9	1.184	0.551	0.495
Nu-Eu	−15.89	−1.00	2.58	2.19	0.068	0.003	34	1.089		

Rif, Betics and Alboran Region

Seismicity here is distributed along a ∼300 km wide, roughly SW-NE trending region, that joins the southwestern Iberia and northern Algeria compressive segments of the plate boundary, forming a 'Z-shaped' deformation zone (Figs 2 and 3). Focal solutions display a larger variety of faulting mechanisms, with respect to the adjacent segments of the plate boundary, although extensional to strike-slip faulting prevail (Figs 4a and b).

In particular, a mainly transcurrent tectonic regime characterizes the Rif, with *P*-axes oriented N25°W to N–S, suggesting a left-lateral component of motion along a NE–SW oriented fault system. The Alboran and Betics are mainly characterized by strike-slip and tensional to transtensional regimes (Fig. 4b), with T-axes mainly N75°E oriented (Fig. 4c). The relative motion between stations in Morocco and southern Iberia (i.e. IFRN, RABT, TETN and SFER) and stations in Algeria and NE-Betics (i.e. ARZE, ALAC) provides an upper bound of the ∼E–W extension possibly accommodated in the Alboran-Betics region, which is of the order of 2.1 ± 0.7 mm yr^{-1}.

Clearly, deformation in this part of the plate boundary cannot be easily explained in terms of simple Africa-Eurasia plate convergence, therefore, suggesting that deep dynamic processes may control the deformation at the surface. Actually, subcrustal earthquakes (35–150 km), sometimes as deep as 600 km, are present in this region (Fig. 2). This deep seismicity has been interpreted as related to a remnant lithospheric body, E-ward dipping in the mantle beneath southern Iberia (Blanco & Spakman 1993; Piromallo

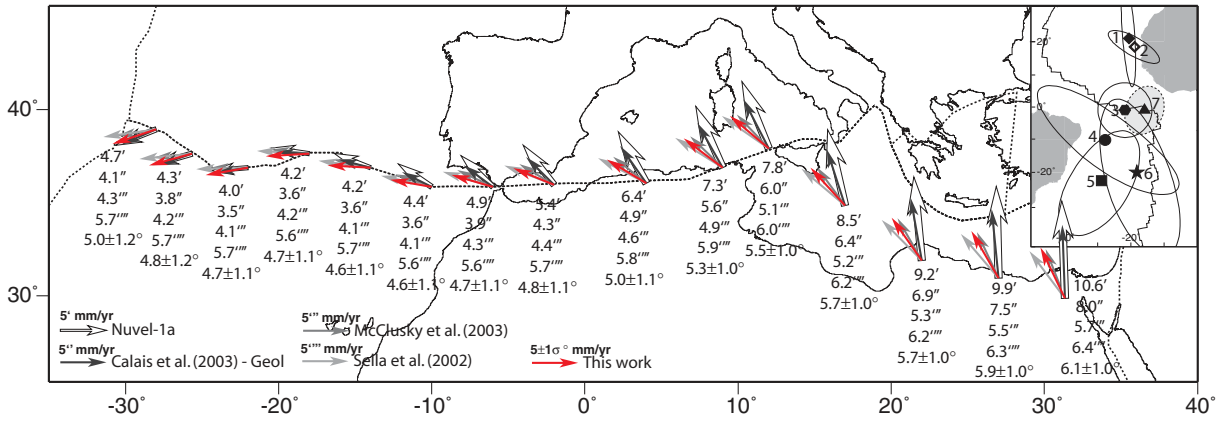

Figure 5. Africa-Eurasia kinematic boundary conditions predicted by geologically and some geodetically derived relative Euler poles, along a simplified plate boundary (dashed line). Arrows and numbers show the displacement vectors and rates (in mm yr^{-1}) of the African plate with respect to the Eurasia plate (1σ uncertainties are reported for the convergence rates computed in this work). Upper right inset shows the location and error ellipses (at 95% confidence level) of Africa (Nubia)-Eurasia rotation poles from: (1) Nuvel-1A (DeMets *et al*. 1994); (2) Calais *et al*. (2003), geological model; (3) McClusky *et al*. (2003); (4) Calais *et al*. (2003), geodetic model; (5) D'Agostino & Selvaggi (2004); (6) REVEL (Sella *et al*. 2002) and (7) this work.

& Morelli 2003). A variety of geodynamic models have been proposed to explain the tectonic evolution of this region including past or present subduction or delamination of overthickened continental lithosphere (Seber *et al*. 1996; Calvert *et al*. 2000; Gutscher *et al*. 2002).

However, the GPS velocity profile 1 in Figs 8 and 9, constructed across the Gulf of Cadiz, shows that no significant deformation is occurring between the sites located on either sides of the allochthonous units in Morocco (IFRN, RABT and TETN) and southern Iberia (SFER), which are moving coherently (see Figs 6a and 7). This observation suggests that any deformation related to a possible eastward dipping subduction in the Gibraltar region has ceased or significantly slowed down. Instead, GPS data (profile 1^{n} in Figs 8 and 9) indicate that 1.8 ± 0.8 mm yr^{-1} of right-lateral motion are accommodated across the northern limit of the allochthonous units (i.e. between SFER and the stations located north of the Betics FTB). This deformation, that is not clearly expressed by focal mechanisms, can be attributed to strain accumulation across the seismic belt at the southwestern Iberian margin.

The observed about S-ward displacement of stations in Morocco, with respect to the Nubian plate, is also confirmed by Fadil *et al.* (2006), who, adding new campaign GPS data in northern Morocco suggest that delamination and southward rollback of the African lithospheric mantle under the Alboran and Rif domains can be adopted to explain the complex pattern of asymmetric deformation observed in this region.

High, Middle Atlas and Tunisian Atlas

In northern Africa seismicity is mainly distributed in a narrow belt running along the northern Algerian coasts, where the greater values of seismic flux are also reached (Fig. 3). The High Plateau looks almost aseismic, and only some sparse moderate seismicity can be observed along the Saharan Atlas (Figs 2 and 3), whereas south of it seismicity is almost absent. Clusters of scarce to moderate seismicity are present along the SW–NE trending Middle and High Atlas mountain ranges in Morocco, providing a relatively low seismic flux, of the order of $10^{17}/10^{19.5}$ dyne $\times$ cm $\times$ km^{-2} yr^{-1}.

Few focal solutions are available for the Atlas belt, and do not show uniform tectonic regimes, since normal, inverse and strike-slip faulting mechanisms are present. Nevertheless, the orientation of *P*-axes of cumulative moment tensors along the High and Middle Atlas agrees with the predicted direction of Africa-Eurasia convergence (Fig. 4c). Actually, GPS data (profile 2 in Figs 8 and 9) indicates that deformation along the Middle and High Atlas is still active, suggesting that this belt is presently accommodating up to 1.7 ± 0.8 mm yr^{-1} WNW–ESE oriented shortening. Fadil *et al*. (2006), from the analysis of additional campaign GPS data in Morocco observed smaller shortening rates across the Atlas (up to 1 mm yr^{-1}) but larger S-ward displacement rates for stations in the Rif of Morocco. Nevertheless, the values we obtain from the common CGPS stations agree (to the 95% confidence level) with Fadil *et al*. (2006) results. Moreover, Fadil *et al*. (2006) velocities with respect to Nubia for stations located south of the Atlas display insignificant to null residuals, strengthening our choice of combining GPS velocities and Nubia-Eurasia predicted displacements to investigate deformation rates across the plate boundary.

In the Tunisian Atlas seismicity appears to be more frequent (with a seismic flux up to $10^{19.5}$ dyne $\times$ cm $\times$ km^{-2} yr^{-1}), though sparser than along northern Algeria, and few focal mechanisms are available. Here both strike-slip and thrust mechanisms coexist, but the few data do not reveal a predominant tectonic regime. The observed compressional tectonics, with *P*-axes trending from N20°W to E–W (Figs 4a–c), can be tentatively associated to activity of the Tunisian Atlas belt that in this region changes its trend from about E–W to about N–S, according to recent reactivation of blind thrust front bounding the eastern High Atlas to the south (Vially *et al*. 1994).

Tell and Algero-Balearic Basin

In the Algerian Tell, seismicity is mainly concentrated along a relatively narrow belt (between longitude 2°W and 6°E), and is moderate to large in magnitude (e.g. the 1980 El Asnam $M_w = 6.9$ and the Alger May 21, 2003 $M_w = 6.9$ earthquakes). The active seismic deformation is mainly described by a N30°W oriented shortening, with purely compressive and strike-slip tectonic regimes (Figs 4b and c). Profiles 3 and 4 (Figs 8 and 9) show that the Algerian Tell accommodates from 2.7 to 3.9 mm yr^{-1} of the present-day Nubia-Eurasia convergence. P-axes in this region are 30° clockwise rotated with respect to the predicted plate convergence direction (see Fig. 4c), suggesting a partitioning of the Nubia-Eurasia convergence into a

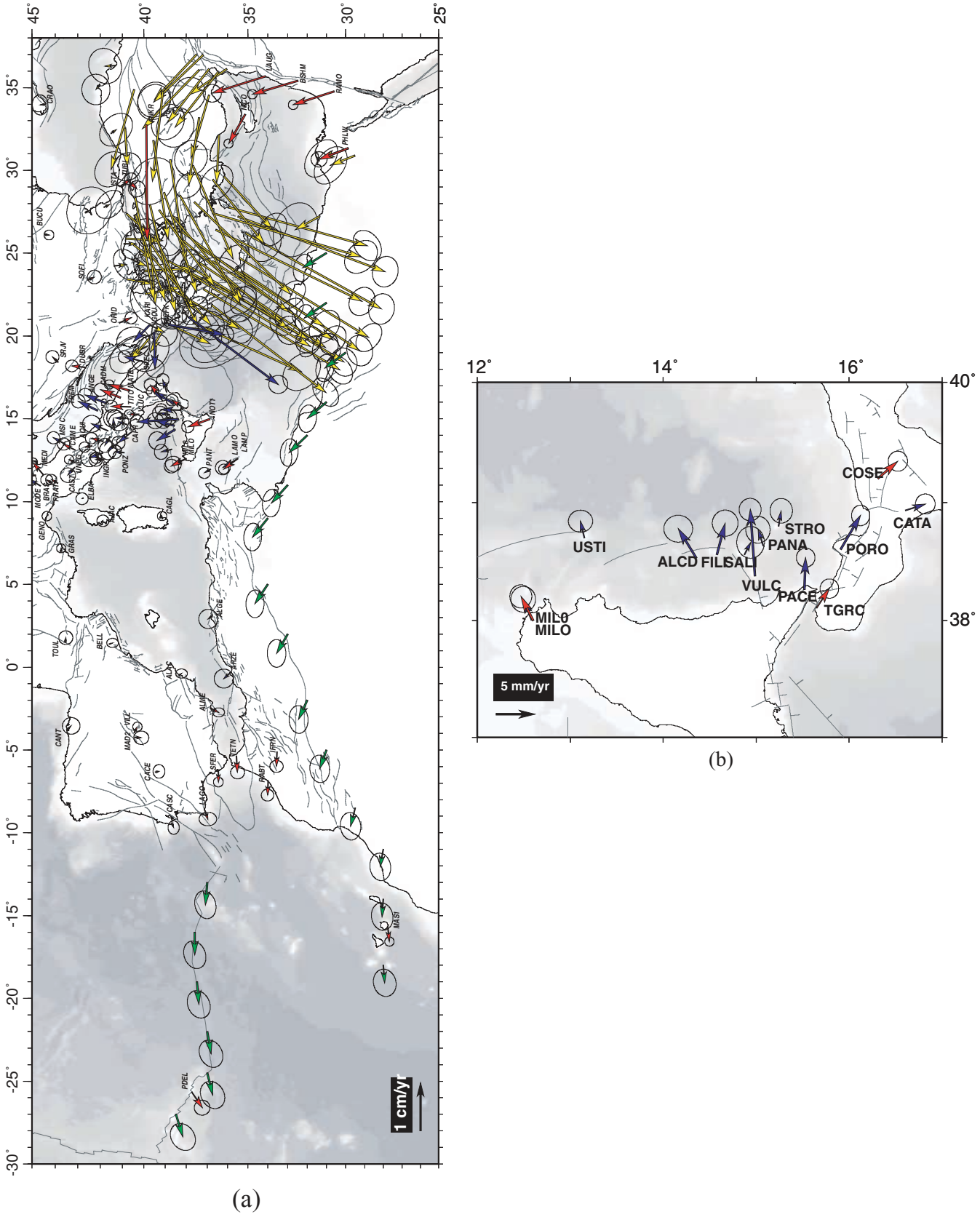

Figure 6. (a and b) Horizontal velocities (with 95% error ellipses) given with respect to the Eurasian plate. Red arrows: permanent GPS stations; blue arrows: non-permanent GPS stations; yellow arrows: subset of McClusky *et al*. (2000) velocity field transformed into the Eurasian fixed frame computed in this work. Green arrows display the motion vectors of points south of the seismically active belts in northern Africa predicted by the Nubia-Eurasia Euler vector obtained in this work.

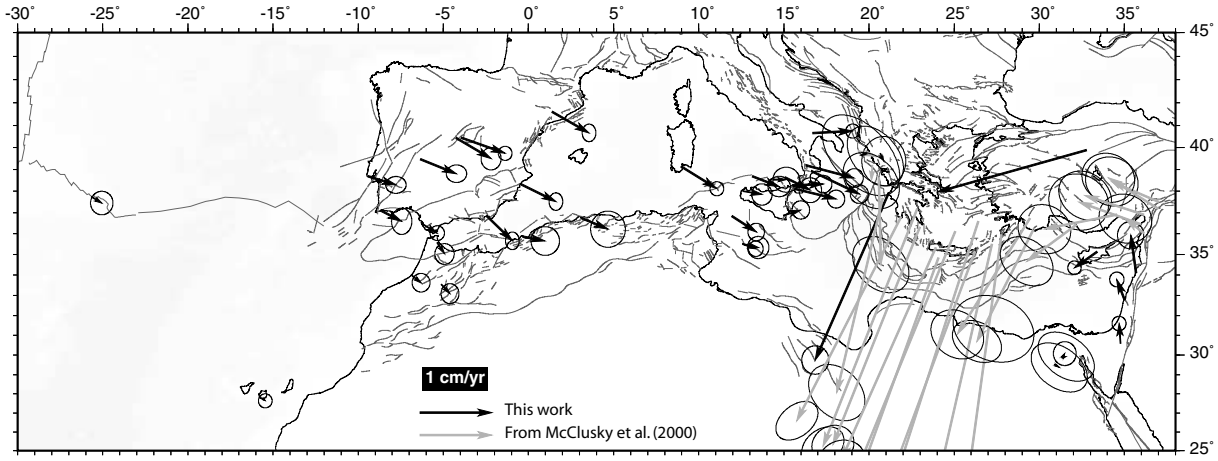

Figure 7. Velocities (with 95% error ellipses) of stations along the Nubia-Eurasia plate boundary given with respect to our Nubian fixed reference frame (see Table 2). Black arrows: GPS velocities obtained in this work; grey arrows: GPS velocities from McClusky *et al*. (2000) transformed into our Nubian fixed reference frame.

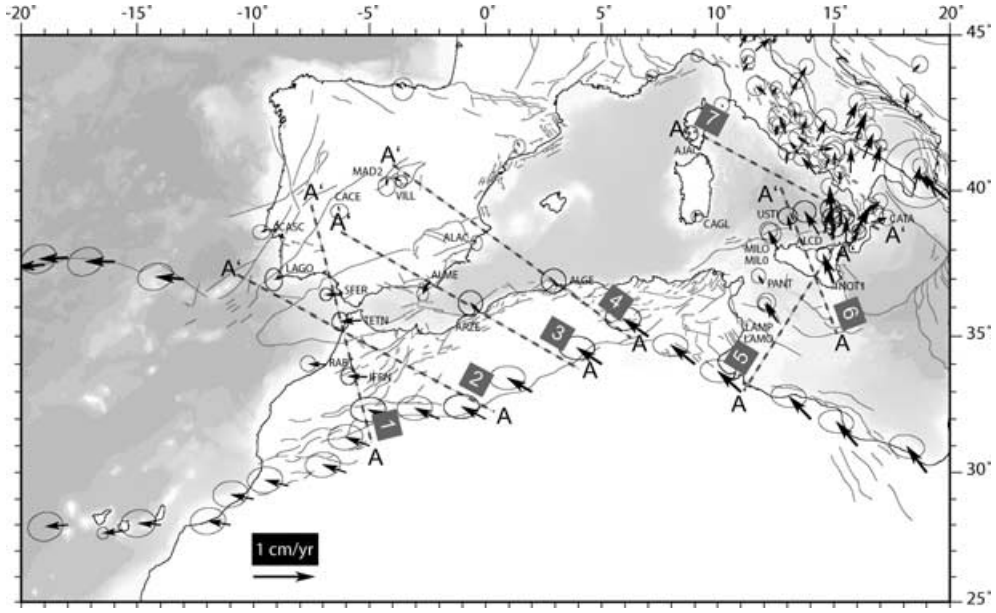

Figure 8. Scheme of the GPS velocity profiles drawn to compute the deformation rates across the Nubia-Eurasia plate boundary deformation zone. Velocities are plotted in each profile from A to A′.

compressional and a right-lateral strike-slip component, which is supported by the occurrence of strike-slip events (Figs 4a and b) and the residual motion of ARZE and ALGE stations with respect to Nubia (Fig. 7). These observations are in agreement with neotectonic data from Morel & Meghraoui (1996) who interpreted this segment of the plate boundary as a transpressive deformation zone, where active thrust faults are controlled by right-lateral transcurrent faults.

In the Algero-Balearic basin significant seismicity (Figs 2 and 3) occurs only offshore northern Algeria and southern Spain (i.e. west of the Balearic Islands), displaying compressive tectonic regimes with P-axes oriented N15W° to N30°W (Figs 4a–c). The observed active thrust faulting offshore northern Algeria is in agreement with other seismological and geophysical data (Déverchére *et al*. 2005; Domzig *et al*. 2006). Moreover, in agreement with these observations and with geological evidences of active faulting offshore southern Spain (Gràcia *et al*. 2006), GPS data show that active shortening, at rates ranging between 1.6 and 2.7 $\pm$ 0.6 mm yr^{-1}, is occurring between northern Africa and Iberia, across the Algero-Balearic basin (see Figs 6(a), 7 and GPS velocity profiles 3 and 4 in Figs 8 and 9). This result suggests that the Africa-Eurasia convergence is not fully absorbed across the northern Africa seismic belts, but transferred and accommodated northward.

Toward the east, along the Tunisian part of the Tell mountain range, seismicity becomes sparser and scarcer, with moderate to small events (Figs 2 and 3), and the few focal mechanisms available display a transtensional to extensional tectonic regime.

Strait of Sicily, Tunisian-Pelagian Plateau and Libya

The Sardinia Channel and the Strait of Sicily interrupt the continuity of the northern Africa seismic belt. Seismicity in the Pelagian Shelf, actually, is scarce and of small to moderate magnitude. Moderate to

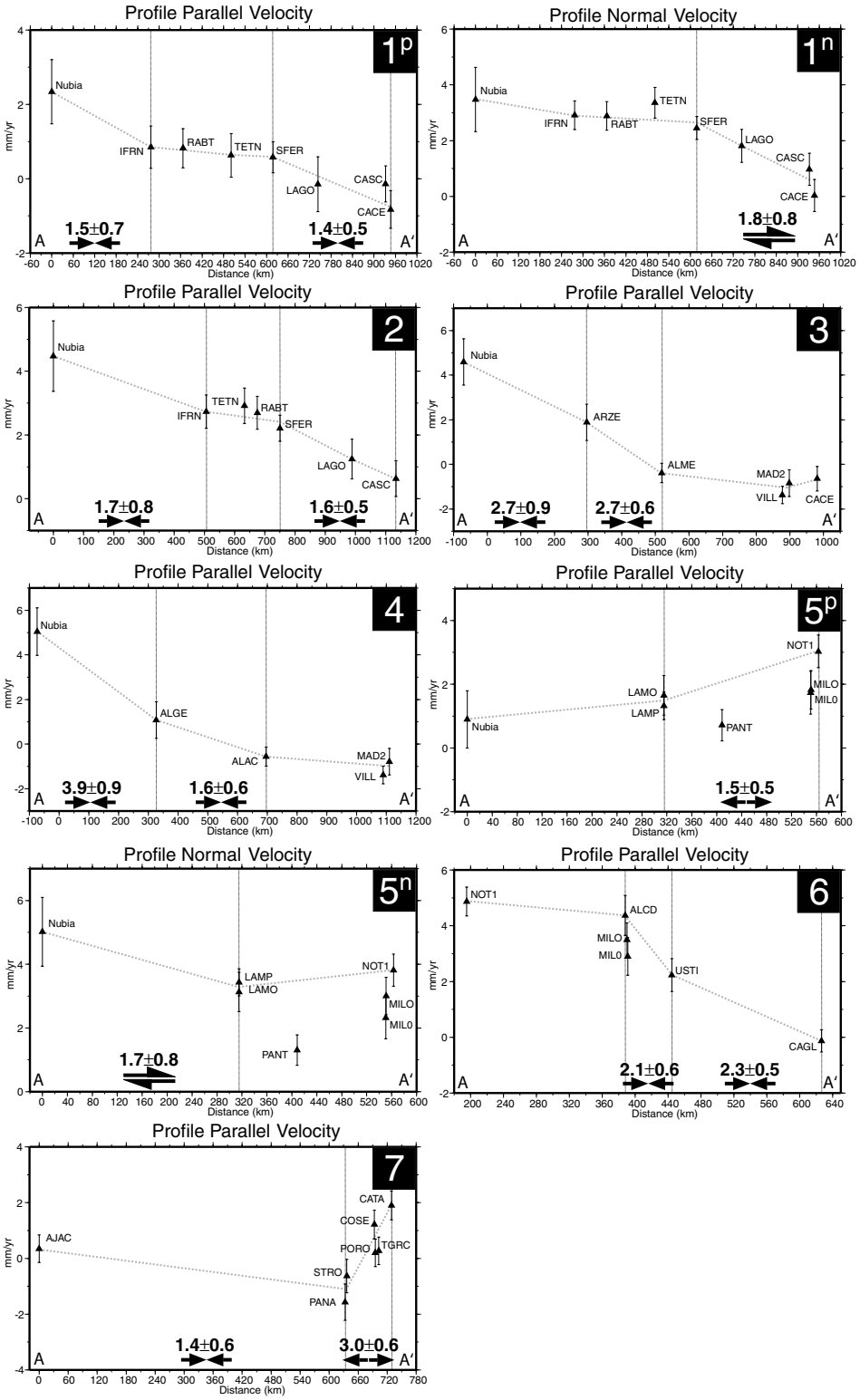

Figure 9. GPS velocity profiles. Diverging arrows show extending regions, converging arrows show regions undergoing active shortening, opposite arrows show regions undergoing strike-slip movements. Rates and uncertainties are in mm yr^{-1}, the horizontal scale is in Km.

large seismicity is present in the Malta plateau and in the Sirt Gulf (Figs 2 and 3).

On the contrary, the map of the seismic flux (Fig. 3) identifies a NW–SE striking, rather diffuse, seismic belt, characterized by moderate to large events that display a clear kinematic coherence. The active tectonic regime derived for this belt is transcurrent (Figs 4a and b), with a right-lateral component of motion along a NW-SE striking fault system. *P*-axes are mainly oriented in agreement with the predicted Nubia-Eurasia plate motion (Fig. 4c). These observations can be reconciled with a strike-slip reactivation of the system

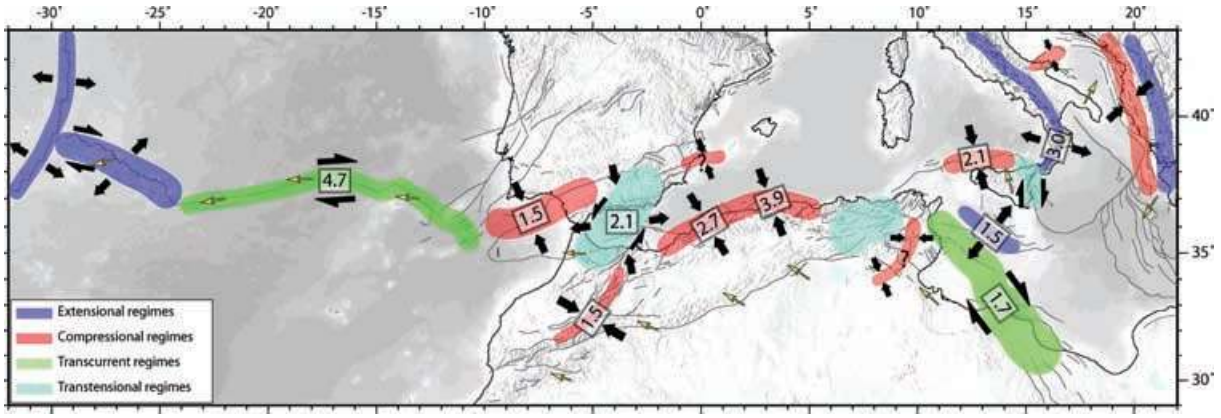

Figure 10. Sketch of the major kinematics and tectonics features of the Nubia-Eurasia plate boundary derived in this work. Deformation rates are in mm yr^{-1}.

of WNW–ESE to NNW–SSE Cretaceous grabens that extends from the Pelagian Shelf to the Sirt Gulf and onshore Libya (Jongsma *et al*. 1985; van der Meer & Cloetingh 1993). On the contrary, along the Pantelleria-Linosa rift system, seismicity is scarce to absent, with the exception of a few strike-slip events near the island of Malta.

The velocity of Lampedusa (LAMP and LAMO stations) indicates a partially independent motion of the Pelagian domain with respect to the Nubian plate (Fig. 7). The GPS velocity cross section number 5^{p} (Figs 8 and 9), which is perpendicular to the NW–SE trending strike-slip seismic belt and to the Strait of Sicily rift system, constrains the active deformation in this region, where seismicity cannot provide a clear picture. The profile-normal GPS velocities (profile 5^{n} in Figs 8 and 9) show a right-lateral motion of 1.7 ± 0.8 mm yr^{-1} between stable Nubia and Lampedusa, which is in agreement with the observed seismically deforming belt running through Libya, west of the Sirt Gulf. The profile-parallel GPS velocities identify a NE-SW oriented extension between Lampedusa and Sicily, that reaches its maximum between LAMP and NOT1, of the order of 1.5 ± 0.5 mm yr^{-1}. The observed extension can be associated with the activity of the Sicily Strait rift system, where high heat flow (Della Vedova *et al*. 2001) may cause deformation to occur aseismically.

Sicily and Southern Tyrrhenian Sea

GPS velocities located on land Sicily (i.e. NOT1, MILO and MIL0 stations) indicate that this domain is moving relative to the Nubian plate (Fig. 7), thus suggesting a microplate like behaviour of Sicily, in agreement with the presence of a decoupling zone corresponding to the distributed deformation between Tunisia and Sicily described in the previous paragraph. In the Southern Tyrrhenian Sea shallow seismicity is well clustered along an ∼E–W trending belt, running between longitude 11°E and 15°E (Figs 2 and 3), and displays seismotectonic features that are similar to those observed along the northern Algeria segment of the plate boundary. East of the central Aeolian islands (roughly corresponding to the Salina-Lipari-Vulcano lineament) shallow seismicity becomes almost absent and deep earthquakes (Fig. 2) are present along an approximately continuous NE–SW striking and NW-ward dipping narrow Benioff plane, that can be followed down to about 600 km (Wortel & Spakman 2000; Piromallo & Morelli 2003; Chiarabba *et al*. 2005).

Focal solutions of shallow earthquakes offshore northern Sicily are highly consistent, and outline a narrow compressive belt, with P-axes oriented from N–S to N20°W, in agreement with the motion of Sicily with respect to Eurasia, which differs from the motion of the Nubian plate as clearly shown in Fig. 4c. The GPS velocity profile 6 (Figs 8 and 9) shows that no active shortening is occurring between NOT1 and ALCD, in agreement with earthquakes distribution in Sicily and observations of Late Pleistocene sediments sealing the thrust front (Argnani 1987; Patacca & Scandone 2004). Although some younger out-of-sequence thrusting has been reported on land (Lickorish *et al*. 1999), the distribution of available GPS stations may not be able to catch this deformation. On the contrary, GPS data (Fig. 8) show that 2.1 ± 0.6 mm yr^{-1} of the NW-ward drift of Sicily (occurring at ∼4 mm yr^{-1}) are accommodated across the southern Tyrrhenian seismic belt. The residual shortening, corresponding to 2.3 ± 0.5 mm yr^{-1}, is likely to be accommodated northward, between Ustica (USTI station) and the Corsica-Sardinia block. Although few compressive earthquakes are present in the southern Tyrrhenian basin (e.g. offshore northeastern Sardinia, Fig. 4a), active thrusting has been observed offshore Liguria (Larroque *et al*. 2001), suggesting that compression may be transferred northward across the rigid Tyrrhenian block. Although this result is principally based on the non-permanent GPS stations at Ustica, it is worth noting that its velocity is well constrained, being obtained using data from nine different surveys between 1994 and 2003 (see Serpelloni *et al*. 2002 and Serpelloni *et al*. 2005 for more details).

The central Aeolian region marks an abrupt change in both GPS velocities and seismotectonics (Pondrelli *et al*. 2004b). East of the Alicudi Island (ALCD station), in fact, velocities undergo a progressive clockwise rotation (Fig. 6b), that in Calabria turn NE-ward. Moreover, a high velocity (i.e. ∼50% larger than the most rapid surrounding stations FILI, ALCD and PACE) characterize the Island of Vulcano (VULC) and comparable rates and directions are also observed in northeastern Sicily (Hollestein *et al*. 2003). These 'anomalous' velocities, (significantly higher than the predicted plate convergence rate), are likely due to a superposition of effects related to the presence of a complex tectonic framework accommodating the continental collision-to-subduction transition (D'Agostino & Selvaggi, 2004; Goes *et al*. 2004; Pondrelli *et al*. 2004b; Govers & Wortel 2005).

East of Alicudi, thrust mechanisms do not prevail (Fig. 4a), while extensional to strike-slip mechanisms occur along a nearly NNW–SSE alignment, which connects the central Aeolian Islands to Mount Etna, and continues toward the south along the eastern Sicily

escarpment (see also Musumeci *et al*. 2005). The seismotectonic setting of this area is characterized by a transtensional to strike-slip regime (Fig. 4b), with T-axes E–W to N60°E oriented (Fig. 4c). It is worth noting that a single structure that carries all this deformation does not exist, and GPS velocities in Calabria and eastern Aeolian Islands suggest a region of distributed deformation that is likely to accommodate a combined extensional and right-lateral kinematics. The velocities of PACE, in northeastern Sicily and TGRC, in Calabria, provide a value of 2.0 ± 0.5 mm yr^{-1} for the active extension across the Messina Strait, oriented about perpendicularly to the 1908 seismic source (Valensise & Pantosti 2001).

Calabrian Arc

In Calabria the number of instrumental earthquakes is smaller and the pattern of seismic deformation is less defined than adjacent domains (particularly for the external Calabrian Arc), although large events (mainly extensional) cause high values of the seismic flux on land (Figs 3 and 4a). The active tectonic regime in Calabria is characterized by a strike-slip to NW–SE oriented extension, with T-axes about perpendicular to the chain axis, suggesting that the dominance of compression driven by the Nubia-Eurasia plate convergence no longer holds there (Figs 4a–c).

The GPS velocity profile 7 (Figs 8 and 9), running from the Corsica-Sardinia block to the Calabrian arc, shows that there are no evidences of active extension in the Tyrrhenian basin. On the contrary, a NW–SE shortening (at a level of 1.4 ± 0.6 mm yr^{-1}) is likely to be accommodated there. The whole NW–SE extension affecting the Calabrian arc is of the order of 3.0 ± 0.6 mm yr^{-1}, 2.0 mm yr^{-1} of which are accommodated on land.

All these observations suggest that the rollback in the Tyrrhenian-Calabrian system is almost stopped or significantly slowed down. However, the particular geography of the region (i.e. the distribution of land and seas), the few GPS stations in Calabria and the lack of stations in the Ionian Sea, leave some uncertainties. In particular, the kinematics of the Ionian basin is a key information missing to define the kinematics of the Ionian-Calabria-Tyrrhenian subduction system, since the absence of GPS stations (no islands are present here) and the few focal solutions in the Calabrian wedge do not provide a well defined pattern of deformation.

The SE-ward displacements of Calabrian stations with respect to Nubia (Fig. 7), occurring at rates of $\sim$6/7 mm yr^{-1}, and the lack of instrumentally recorded thrust earthquakes in the external Calabrian Arc may suggest that convergence is still occurring and that the subduction fault plane may be presently locked (e.g. Gutscher *et al*. 2006). Alternatively, the Ionian basin may be presently moving independently, or partially independently, from the Nubian plate, as already observed in this work for the Pelagian-Sicily region, with important implication for the study of the kinematics and geodynamics of the Central Mediterranean.

Supporting the latter hypothesis, the NE-ward drift of Calabrian stations with respect to Eurasia has been interpreted by Goes *et al*. (2004) in the framework of recent plate reorganization, causing the Calabrian and Ionian domains to be coupled and driven E-ward by the Hellenic slab pull. D'Agostino & Selvaggi (2004), also, proposed the existence of a Calabrian forearc sliver, caused by partitioning of plate convergence along the Calabrian Arc, or, alternatively, of the presence of an independent Ionian block, intermediate between the Nubian and Adriatic plates. The presence of an Ionian microplate, rotating counterclockwise with respect to Nubia, around a pole located in Libya, has been already proposed by Westaway (1990). However, it is worth noting that in Calabria the regional uplift (Bordoni & Valensise 1998) could have promoted gravitational instability within the orogenic wedge, particularly towards low topographic areas, such as the deep Ionian basin, causing graben formation and clockwise rotations (Argnani 2000), suggesting that the velocity field in Calabria could not be taken as fully representative of the kinematics of the Ionian region.

DISCUSSION AND CONCLUSIONS

Using seismological and GPS data, and taking into account the geology of the study area, we summarize the observed kinematic and tectonic features of the Western Mediterranean Africa-Eurasia plate boundary through a map that outlines the main deforming zones with the prevailing active tectonic regimes and the measured deformation rates (Fig. 10). The spatial distribution of instrumental seismicity (Fig. 2), analysed in terms of crustal seismic flux (Fig. 3), outlines the major seismogenic zones. Earthquake focal mechanisms, analysed in terms of seismic moment summation (Fig. 4a), allow us to identify segments of the plate boundary characterized by relatively homogeneous tectonic regimes (Fig. 4b), and to define the kinematics of seismic deformation (Fig. 4c). The Nubia-Eurasia Euler vector (Fig. 5) and the combined GPS velocity field (Figs 6a and b) provide additional constraints about the kinematics and rates of deformation across the plate boundary (Fig. 9).

Our results evidence a fragmentation of the compressive plate boundary, which is interrupted by regions characterized by a more distributed deformation and less homogeneous tectonic regimes, although mainly strike-slip to extensional. Along the broader African-European deformation zone, that extends between latitude 30°N and 40°N (Fig. 2), we identify three mainly compressive belts, where deformation appears more localized: (i) southwestern Iberia, (ii) northern Algeria and (iii) southern Tyrrhenian. We also identify three main breaks separating them: (i) the Rif-Alboran-Betics region; (ii) the region encompassing the Sardinia Channel, northern Tunisia and the Strait of Sicily and (iii) eastern Sicily. These breaks occur in areas where tectonic structures with different trends interfere (e.g. the Tell and Atlas in Tunisia). In correspondence of the observed breaks we find deforming belts (i.e. the High and Middle Atlas, the Tunisian Atlas and the offshore Tunisia-Libya belt) that extend from the plate boundary into the Nubian plate, along preexisting tectonic lineaments. An important result of our analysis is that GPS data, according to earthquake focal mechanisms, evidence an independent motion of the Pelagian-Sicilian domain that contributes to the complexity of the Central Mediterranean kinematic and tectonic setting.

In northwestern Africa and southern Iberia plate convergence is partially absorbed across the Middle and High Atlas ($\sim$1.5 mm yr^{-1}) and transferred northward to the southwestern Iberia compressive belt (see Figs 8 and 9), which connects the oceanic transform to the continent and accomodates $\sim$1.5 mm yr^{-1} of NW–SE compression. The NE–SW trending Rif-Alboran-Betics belt, where deformation appears distributed over a wider region and mainly characterized by strike-slip to extensional tectonic regimes, joins the compressive south Iberia segment of the plate boundary with the FTB of north Africa. The tectonic and kinematic features observed in this region are difficult to explain in the context of simple plate convergence, suggesting that deep dynamic processes may be responsible for the observed complexity. In any event, data across the Gibraltar Arc suggest that any deformation associated to a possible E-ward dipping subduction is stopped or significantly slowed down, requiring other

processes to explain surface observations (e.g. Fadil *et al*. 2006). GPS data, moreover, provide an upper bound for the observed regional E-W oriented extensional deformation across the Alboran basin of the order of ∼2 mm yr^{-1}.

While the Saharian Atlas appears almost aseismic and few focal mechanisms indicates active thrusting only along the Tunisian Atlas segment, the Algerian Tell represents the compressive segment of the plate boundary with the highest deformation rates, accomodating up to ∼3.9 mm yr^{-1} of plate convergence across a relatively narrow deformation zone. Here convergence, according to neotectonic data (Morel & Meghraoui, 1996), appears partitioned into a N30°W compression and a strike-slip (right-lateral) deformation. Moreover, our data indicate that residual shortening (between 1.6 and 2.7 mm yr^{-1}) is likely to be accomodated northward (i.e. in the Algerian basin and southern Spain; see Figs 8 and 9), and even if such a deformation is less well constrained by seismic data, it is in agreement with recent geological and geophysical observations (e.g. Déverchére *et al*. 2005; Gracia *et al*. 2006).

The poorly constrained and distributed transtensional deformation in northern Tunisia (Fig. 3) separates the northern Africa and southern Tyrrhenian compressive plate boundary segments. East of longitude 10°E the presence of a region of distributed deformation, accommodating ∼1.7 mm yr^{-1} of right-lateral motion across the NW–SE trending Tunisia-Libya belt, and ∼1.5 mm yr^{-1} of NE–SW extension across the Strait of Sicily, allows for a relatively independent motion of the Pelagian and Sicilian domains with respect to the surrounding major plates (i.e. Nubia and Eurasia).

The southern Tyrrhenian compressive belt accommodates ∼2.1 mm yr^{-1} of the NW-ward drift of Sicily (Fig. 6b). Residual shortening, at a level of ∼2.3 mm yr^{-1}, is likely to be accomodated northward in the Tyrrhenian basin, although compression is not clearly evidenced by seismicity. The ∼N–S trending transtensional belt running along eastern Sicily and the Iblean-Maltese Escarpment (Argnani & Bonazzi 2005) represents the transition zone between the 'Northern Africa' plate boundary domain (represented here by the south Tyrrhenian seismic belt) and the Calabria-Apennine region, dominated by extension. This belt accommodates right-lateral and extensional deformation through a complex pattern of tectonic structures (including the Tindari-Giardini and Messina Strait faults), and shows rapid movements of some GPS stations in NE-Sicily and Aeolian Islands region (e.g. Hollenstein *et al*. 2003; Goes *et al*. 2004). GPS data across the Tyrrhenian-Calabrian subduction zone suggest that slab rollback has almost stopped or significantly slowed down, while ∼3.0 mm yr^{-1} of NW-SE extension occurs across Calabria. Unfortunately, the kinematics of the Ionian basin is not known, and the few focal mechanisms available do not provide useful constraints.

The orientation of *P*-axes in the study region, roughly corresponding to the direction of plate convergence for large part of plate boundary zone (Fig. 4c), suggests that, outside pre-existing local heterogeneities, the present-day tectonic and kinematic setting is still mainly controlled by the Nubia-Eurasia plate convergence. It is only east of the central Aeolian Islands (i.e. the Salina-Lipari-Vulcano lineament) that the observed deformation pattern is no more directly related to plate convergence. Along the Calabrian Arc and Apennines, in fact, the contribution of the subducting Ionian oceanic lithosphere, and the counterclockwise rotation of the Adriatic domain (w.r.t. Eurasia; e.g. Battaglia *et al*. 2004; Nocquet & Calais, 2004), appear to greatly affect the observed kinematics and tectonic regimes.

A unique geodynamic interpretation of the observed surface kinematics and tectonics seems difficult. However, the presence along the plate boundary of zones of more complex composite tectonic regimes (mainly strike-slip to tensional) can be correlated with other geophysical and geological observations. In particular, these breaks occur over discontinuities already detected by seismic tomography (Wortel & Spakman, 2000; Piromallo & Morelli 2003; Pondrelli *et al*. 2004b; Lucente *et al*. 2006). These sectors recorded complex geodynamic processes during the evolution of the Western Mediterranean subduction system (e.g. Carminati *et al*. 1998; Argnani 2000; Faccenna *et al*. 2004; Fullea *et al*. 2006; Lucente *et al*. 2006), which shaped the geometry of the retreating arcs. These observations suggest that deep dynamics, combined with inherited structural crustal heterogeneities, may be responsible for the observed tectonics and kinematics. The new picture obtained in this work can provide additional constraints for the development of geodynamic models that address the problem of studying the processes that are driving the current plate interactions and crustal tectonic complexities in the Mediterranean region.

ACKNOWLEDGMENTS

This work was partially funded by the Italian Space Agency (ASI), by the Ministry of Public Education, University and Research, by the Department of Civil Protection. We are thankful to all individuals and institutions contributing in the GPS field surveys. Thanks are due to ASI-CGS in Matera, EUREF, UNAVCO and SOPAC for providing CGPS data and solutions. The authors thank Roland Bürgmann and Daniel Stich for constructive discussions and comments. Comments and reviews from Editor and two anonymous reviewers greatly improved the quality of the manuscript. The maps have been created using the Generic Mapping Tools (GMT) software (Wessel & Smith 1995).

REFERENCES

Altamimi, Z., Sillard, P. & Boucher, C., 2002. ITRF2000: a new release of the international terrestrial reference frame for earth science applications, *J. Geophys. Res.,* **107**(B10), 2214, doi:10.1029/2001JB000561.

Alvarez-Marron, J., 1999. Pliocene to Holocene structure of the eastern Alboran Sea (Western Mediterranean), in *Proceedings of the Ocean Drilling Program, Scientific Results*, Vol.161, 345–355.

Anderson, J. E., 1996. The Neogene structural evolution of the western margin of the Pelagian Platform, central Tunisia, *J. Struct. Geol.*, **18**, 819–833.

Argnani, A. & Bonazzi, C., 2005. Tectonics of eastern sicily offshore, *Tectonics*, **24**, TC4009, doi:10.1029/2004TC001656.

Argnani, A. & Savelli, C., 1999. Cenozoic volcanism and tectonics in the southern Tyrrhenian: space-time distribution and geodynamic significance, *J. Geodyn.*, **27**, 409–432.

Argnani, A., 1987. The Gela Nappe: evidence of accretionary melange in the Maghrebian foredeep of Sicily, *Mem. Soc. Geol. It.*, **38**, 419–428.

Argnani, A., 1990. The Strait of Sicily Rift Zone: foreland deformation related to the evolution of a back-arc basin, *J. Geodyn.*, **12**, 311–331.

Argnani, A., 2000. The Southern Tyrrhenian subduction system: recent evolution and neotectonic implications, *Ann. Geofis.*, **43**(3), 585–607.

Argnani, A., 2005. Possible record of a Triassic ocean in the southern Apennines, *Boll. Soc. Geol. It.*, **124**, 109–121.

Banks, C. J. & Warburton, J., 1991. Mid-crustal detachment in the Betic system of southern Spain, *Tectonophysics*, **191**, 275–289.

Battaglia, M., Murray, M. H., Serpelloni, E. & Bürgmann, R., 2004. The Adriatic region: an independent microplate within the Africa-Eurasia collision zone, *Geophys. Res. Lett*., **31**(9), L09605, 10.1029/2004GL019723.

Benaouali-Mebarek, N., Frizon de Lamotte, D., Roca, E., Bracene, R., Faure, J. L., Sassi, W. & Roure, F., 2006. Post-Cretaceous kinematics of the Atlas and Tell systems in central Algeria: early foreland folding

and subduction-related deformation, *C. R. Geoscience*, **338**, 115–125, doi:10.1016/j.crte.2005.11.005.

Biju-Duval, B., Le Quellec, P., Mascle, A., Renard, V. & Valery, P., 1982. Multibeam bathymetric survey and high resolution seismic investigations on the Barbados Ridge complex (Eastern Caribbean): a key to the knowledge and interpretation of an accretionary wedge, *Tectonophysics*, **86**, 275–304

Blanco, M. J. & Spakman, W., 1993. The P-wave velocity structure of the mantle below the Iberian peninsula: evidence for subducted lithosphere below southern Spain, *Tectonophysics*, **221**, 13–34.

Blankenship, C. L., 1992. Structure and paleogeography of the External Betic Cordillera, Southern Spain, *Mar. Petrol. Geol.*, **9**, 256–264.

Blewitt, G., Bock, Y. & Gendt, G., 1993. *Regional Clusters and Distributed Processing*, IGS Analysis Center Workshop, Ottawa, Canada, pp. 62–91.

Boccaletti, M., Cello G. & Tortorici, L., 1987. Transtensional tectonics in the Sicily Channel, *J. Struct. Geol.*, **9**, 869–876.

Bonardi, G., Cavazza, W., Perrone, V. & Rossi, S., 2001. Calabria-Peloritani terrane and Northern Ionian Sea, in *Anatomy of a Mountain: The Apennines and Adjacent Mediterranean Basins*, pp. 287–306, eds Vai, G. B. & Martini, I. P., Kluwer Academic Publisher, London.

Bordoni, P. & Valensise, G., 1998. Deformation of the 125 ka marine terrace in Italy: tectonic implications, in *Coastal Tectonics, Geol. Soc. London Spec. Publ.*, Vol.146, pp. 71–110, eds Stewart, I.S.. & Vita Finzi, C., Geological Society, London.

Braunmiller, J., Kradolfer, U. & Giardini, D., 2002. Regional moment tensor determination in the European-Mediterranean area – initial results, *Tectonophysics*, **356**, 5–22.

Carminati, E., Wortel, M. J. R., Spakman W. & Saladini, R., 1998. The role of slab detachment processes in the opening of the western-central Mediterranean basin: some geological and geophysical evidences, *Earth Planet. Sci. Lett.*, **160**, 651–665.

Calais, E., DeMets, C. & Nocquet, J. M., 2003. Evidence for a post-3.16-Ma change in Nubia-Eurasia-North America plate motions? *Earth. Plan. Sci. Lett.*, **216**, 8–92.

Calvert, A.*et al.,* 2000. Geodynamic evolution of the lithosphere and upper mantle beneath the Alboran region of the western Mediterranean: constraints from travel time tomography, *J. Geophys. Res.*, **105**(B5), 10 871–10 898, doi:10.1029/2000JB900024.

Catalano, R., Doglioni, C. & Merlini, S., 2001. On the Mesozoic Ionian Basin, *Geophys. J. Int.*, **144**, 49–64.

Chalouan, A., Michard, A., Feinberg, H., Montigny, R. & Saddiqi, O., 2001. The Rif mountain building (Morocco): a new tectonic scenario, *Bull. Soc. Geol. Fr.*, **172**, 603–616.

Chiarabba, C., Jovane, L. & Di Stefano, R., 2005. A new view of Italian seismicity using 20 yr of instrumental recordings. *Tectonophysics*, **395**, 251–268.

Comas, M. C., Platt, J. P., Soto, J. I. & Watts, A. B., 1999. The origin and tectonic history of the Alboran basin: insights from leg 161 results, *Proc. Ocean Drill. Program Sci. Results*, **161**, 555–579.

D'Agostino, N. & Selvaggi, G., 2004. Crustal motion along the Eurasia-Nubia plate boundary in the Calabrian Arc and Sicily and active extension in the Messina Straits from GPS measurements, *J. Geophys. Res.*, **109**, B11 402, doi:10.1029/2004JB002998.

De Voogd, B. *et al.* 1991. First deep seismic reflection transect from the Gulf of Lions to Sardinia (ECORS-CROP Profiles in Western Mediterranean), in *Continental Lithosphere: Deep Seismic Reflections, Am. Geophys. Union. Geodyn. Ser.*, Vol.22, pp. 265–274, eds Meissner, R., Brown, L., Durbaum, H.J., Franke, W., Fuchs K. & Seifert, F., American Geophysical Union, Washington.

Della Vedova, B., Bellani, S., Pellis, G. & Squarci, P., 2001. Deep temperatures and surface heat flow distribution, in *The Apennines: Anatomy of an Orogen*, pp 65–76 + 2 maps, eds Vai, G. B. & Martini, P., Kluwer Academic Publishers, Dordrecht.

DeMets, C., Gordon, R. G., Argus, D. F., & Stein, S., 1994. Effect of recent revisions to the geomagnetic reversal time scale on estimates of current plate motions, *Geophys. Res. Lett.*, **21**, 2191–2194.

Dercourt, J., Ricou, L. E. & Vrielynck, B. (eds), 1993. *Atlas Tethys Palaeonvironmental Maps*, pp 307, 14 maps, 1 pl, Gauthiers-Villars, Paris.

Dèverchère J. *et al.*, 2005. Active thrust faulting offshore Boumerdes, Algeria, and its relations to the 2003 Mw 6.9 earthquake, *Geophys. Res. Lett.*, **32**, L04311, doi:10.1029/2004GL021646.

Dewey, J. F., Pitman, W. C., Ryan, W. B. F. & Bonnin, J., 1973. Plate tectonics and the evolution of the Alpine system, *Bull. Soc. Am. Bull.*, **84**, 3137–3180.

Dewey, J. F., Helman, M. L., Turco, E., Hutton, D. H. W. & Knott, S. D., 1989. Kinematics of the Western Mediterranean, in *Alpine Tectonics*, Vol.45, pp. 265–283, eds Coward, M. P., Dietrich, D. & Park, R. G., Geological Society Special Publication.

Dixon, T. H., Miller, M., Farina, F., Wang, H. & Johnson, D., 2000. Present-day motion of the Sierra Nevada block and some tectonic implications for the Basin and Range province, North American Cordillera, *Tectonics*, **19**(1), 1–24.

Domzig, A. *et al.*, 2006. Searching for the Africa–Eurasia Miocene boundary offshore western Algeria (MARADJA'03 cruise), *C.R. Géoscience*, **338**, 80–91, doi:10.1016/j.crte.2005.11.009.

Dong, D., Herring, T. A. & King, R. W., 1998. Estimating regional deformation from a combination of space and terrestrial geodetic data, *J. Geod.*, **72**, 200–214.

Dong, D., Fang, P., Bock, Y., Cheng, M. K. & Miyazaki, S., 2002. Anatomy of apparent seasonal variation from GPS–derived site position, *J. Geophys. Res.*, **107**, doi:10.1029/2001JB000573.

Duggen, S., Hoernle, K., Van Den Bogaard, P. & Harris, C., 2004. Magmatic evolution of the Alboran region: the role of subduction in forming the Western Mediterranean and causing the Messinian Salinity Crisis, *Earth Planet. Sci. Lett.*, **218**, 91–108.

Dziewonski, A. M., Chou, T. A. & Woodhouse, J. H., 1981. Determination of earthquake source parameters from waveform data for studies of global and regional seismicity, *J. Geophys. Res.*, **86**, 2825–2852.

Dziewonski, A. M. & Maternovskaya, N. N., 2000. Centroid-moment tensor solutions for October-December 1999, *Phys. Earth Planet. Int.*, **121**, 205–221.

Ekström, G. & England, P., 1989. Seismic strain rates in regions of distributed continental deformation, *J. Geophys. Res.*, **94**, 10231–10257.

Faccenna, C., Piromallo, C., Crespo-Blanc, A., Jolivet, L. & Rossetti, F., 2004. Lateral slab deformation and the origin of the western Mediterranean arcs, *Tectonics*, **23**, TC1012, doi:10.1029/2002TC001488.

Fadil, A. *et al.*, 2006. Active tectonics of the western Mediterranean: geodetic evidence for rollback of a delaminated subcontinental lithospheric slab beneath the Rif Mountains, Morocco, *Geology*, **34**, 529–532.

Fernandes, R. M. S., Ambrosius, B. A. C., Noomen, R., Bastos, L., Wortel, M. J. R., Spakman, W. & Govers, R., 2003. The relative motion between Africa and Eurasia as derived from ITRF2000 and GPS data, *Geophys. Res. Lett.*, **30**(16), 1828, doi:10.1029/2003GL017089.

Fernandes, R. M. S., Bastos, L., Miranda, J. M., Lourenço, N., Ambrosius, B. A. C., Noomen, R. & Simons, W., 2006. Defining the plate boundaries in the Azores region, *J. Volc. Geotherm. Res.*, **156**, 1–9.

Frohlich, C., 1992. Triangle diagrams: ternary graphs to display similarity and diversity of earthquake focal mechanisms, *Phys. Earth Planet. Inter.*, **75**, 193–198.

Frohlich, C., 2001. Display and quantitative assessment of distributions of earthquake focal mechanisms, *Geophys. J. Int.*, **144**, 300–308.

Fullea, J., Fernàndez, M. & Zeyen, H., 2006. Lithospheric structure in the Atlantic–Mediterranean transition zone (southern Spain, northern Morocco): a simple approach from regional elevation and geoid data, *C. R. Geoscience*, **338**, 140–151.

Gasperini P. & Ferrari, G., 2000. Deriving numerical estimates from descriptive information: the computation of earthquake parameters, *Ann. Geofis.*, **43**, 729–746.

Goes, S., Giardini, D., Jenny, S., Hollenstein, C., Khale, H. G. & Geiger, A., 2004. A recent tectonic reorganization in the south-central Mediterranean, *Earth. Planet. Scie. Lett.*, **226**, 335–345.

Gomez, F., Beauchamp, W. & Barazangi, M., 2000. Role of the Atlas mountains (northwest Africa) within the African-Eurasian plate boundary zone, *Geology*, **28**, 775–778.

Govers, R. & Wortel, M. J. R., 2005. Lithosphere tearing at STEP faults: response to edges of subduction zones, *Earth Planet. Scie. Lett.*, **236**, 505–523.

Gràcia, E. *et al.,* 2006. Active faulting offshore SE Spain (Alboran Sea): implications for earthquake hazard assessment in the Southern Iberian Margin, *Earth Planet. Scie. Lett.*, **241**, 734–749.

Gutscher, M. A., Malod, J., Rehault, J. P., Contrucci, I., Klingelhoefer, F., Mendes-Victor L. & Spakman, W., 2002. Evidence for active subduction beneath Gibraltar, *Geology*, **30**, 1071–1074.

Gutscher, M. A., Roger, J., Baptista, M. A., Miranda, J. M. & Tinti, S., 2006. Source of the 1693 Catania earthquake and tsunami (southern Italy): new evidence from tsunami modeling of a locked subduction fault plane, *Geophys. Res. Lett.*, **33**, L08 309, doi:10.1029/2005GL025442.

Hanks, T. C. & Kanamori, H., 1979. A moment magnitude scale, *J. Geophys. Res.*, **84**, 2348–2350.

Hayward, A., Watts, A. B., Westbrook G. K. & Collier J. S., 1999. A seismic reflection and GLORIA study of compressional deformation in the Gorringe Bank region, Eastern North Atlantic, *Geophys. J. Int.*, **138**, 831–850.

Herring, T. A., 2004. *GLOBK: Global Kalman Filter VLBI and GPS Analysis Program Version 10.0*, Massachusetts Institute of Technology, Cambridge.

Hollenstein, Ch., Kahle, H. G., Geiger, A., Jenny, S., Goes, S. & Giardini, D., 2003. New GPS constraints on the Africa-Eurasia plate boundary zone in southern Italy, *Geophys. Res. Lett.*, **30**(18), 1935, doi:10.1029/2003GL017554.

Horvath, F., Berckhemer, H., 1982. Mediterranean backarc-basins, in *Alpine.-Mediterranean- Geodynamics,* p. 141–163, eds Berckheimer, H. & Hsü, K., AGU Geodynamics Series, 7.

ISC (INTERNATIONAL SEISMOLOGICAL CENTRE) 2004. On-line bulletin (http://www.isc.ac.uk/), *Bull. Int. Seismol. Cent.* (Thatcham, United Kingdom).

Jackson, J. & Mckenzie, D., 1988. The relationship between plate motions and seismic moment tensors, and the rates of active deformation in the Mediterranean and Middle East, *Geophys. J. Int.*, **93**, 45–73.

Johnston, A. C., 1996. Seismic moment assessment of earthquakes in stable continental regions I. Instrumental seismicity, *Geophys. J. Int.*, **124**, 381–414.

Jongsma, D., Van Hinte, J. E. & Woodside, J. M., 1985. Geologic structure and neotectonics of the north African continental margin south of Sicily, *Mar. Petrol. Geol.*, **2**, 156–179.

Julià, J. & Mejía, J., 2004. Thickness and VP/VS ratio variation in the Iberian crust, *Geophys. J. Int.*, **156**, 59– 72.

Kanamori, H. & Anderson D. L., 1975. Theoretical basis of some empirical relations in seismology, *Bull. Seism. Soc. Am.*, **65**(5), 1073–1095.

Karnik, V., 1996. *Seismicity of Europe and the Mediterranean,* ed. K. Klima., Academy of Sciences of the Czech Republic, Geophysical Institute, 28pp plus earthquake catalogue.

King, R. W. & Bock, Y., 2004. *Documentation for GAMIT GPS Analysis Software, version 10.01*, Massachusetts Institute of Technology and Scripps Institution of Oceanography.

Kiratzi, A. A. & Papazachos, C. B., 1995. Active Crustal Deformation from the Azores Triple Junction to the Middle East, *Tectonophysics*, **243**, 1–24.

Kostrov, V. V., 1974. Seismic moment and energy of earthquakes and seismic flow of rocks, Izv. Acad. Sci. USSR, *Phys. Solid Earth*, **1**, 23–40.

Kreemer, C., Holt, W. E. & Haines, A. J., 2003. An integrated global model of present-day plate motions and plate boundary deformation, *Geophys. J. Int.*, **154**, 8–34.

Larroque, C. *et al.,* 2001. Active and recent deformation at the Southern Alps-Ligurian basin junction, *Netherland J. Geosci.*, **80**, 255–272.

Le Pichon, X., Bergerat, F. & Roulet, M. J., 1988. Plate kinematics and tectonics leading to the Alpine belt formation: a new analysis, *Geol. Soc. Am., Spec. Pap.,* **218**, 111–131.

Lickorish, W. H., Grasso, M., Butler, R. W. H., Argnani A. & Maniscalco, R., 1999. Structural styles and regional tectonic setting of the Gela Nappe and frontal part of the Maghrebian thrust belt in Sicily, *Tectonics*, **18**, 655–668.

Lucente, F. P., Margheriti, L., Piromallo, C. & Barruol, G., 2006. Mapping the long route of the Tyrrhenian slab through the mantle, *Earth Planet. Sci. Lett.*, **241**, 517–529.

Madeira, J. & Ribeiro, A., 1990. Geodynamic models for the Azores triple junction; a contribution from tectonics, in *Alpine Evolution of Iberia and its Continental Margins*, eds Boillot, G.. & Fontbote, J. M., *Tectonophysics*, **184**(3–4), 405–415.

Malinverno, A. & Ryan, W. B. F., 1986. Extension in the Tyrrhenian Sea and shortening in the Apennines as result of arc migration driven by sinking in the lithosphere, *Tectonics*, **5**, 227–245.

Mao, A., Harrison, C. G. A. & Dixon, T.H., 1999. Noise in GPS coordinate time series, *J. Geophys. Res.*, **104**, 2797–2816.

McClusky, S. *et al.*, 2000. Global Positioning System constraints on plate kinematics and dynamics in the eastern Mediterranean and Caucasus, *J. Geophys. Res.*, **105**(B3), 5695–5719.

McClusky, S., Reilinger, R., Mahmoud, S., Ben Sari, D. & Tealeb, A., 2003. GPS constraints on Africa (Nubia) and Arabia plate motions, *Geophys. J. Int.*, **155**, 126–138.

Morel, J. L. & Meghraoui, M., 1996. Goringe-Alboran-Tell tectonic zone; a transpression system along the Africa-Eurasia plate boundary, *Geology*, **24**, 755–758.

Musumeci, C., Patanè, D., Scarfì, L. & Gresta, S., 2005. Stress Directions and shear-Wave Anisotropy: observations from Local Earthquakes in Southeastern Sicily, Italy, *Bull. Seism. Soc. Am.*, **95**(4), 1359–1374, doi:10.1785/0120040108.

Nocquet, J. M. & Calais, E., 2004. Geodetic measurements of crustal deformation in the Western Mediterranean and Europe, *Pure Appl. Geophys.*, **161**, 661–681.

Patacca, E., Sartori, R. & Scandone, P., 1990. Tyrrhenian basin and Apenninic arcs. Kinematic relations since late Tortonian times, *Mem. Soc. Geol. It.*, **45**, 425–451.

Patacca, E. & Scandone, P., 2004. The Plio-Pleisticene thrust belt-foredeep system in the Southern Apennines and Sicily (Italy), *Geology of Itlay*, Special Vol. for IGC 32, Geol. Soc. Italy, 93–129.

Piquet, A., Tricart, P., Guraud, R., Laville, E., Bouaziz, S., Amrhar, M. & Ait, R., 2002. The Mesozoic-Cenozoic Atlas belt (North Africa): an overview, *Geodin. Acta*, **15**, 185–208.

Piromallo, C. & Morelli, A., 2003. *P*-wave tomography of the mantle under the Alpine-Mediterranean area, *J. Geophys. Res.*, **108**(B2), 2065, doi: 10.1029/2002JB001757.

Pondrelli, S., Morelli, A. & Boschi, E., 1995. Seismic deformation in the Mediterranean area estimated by moment tensor summation, *Geophys. J. Int.,* **122**, 938–952.

Pondrelli, S., 1999. Pattern of seismic deformation in the Western Mediterranean, *Ann. Geofis.*, **42**(1), 57–70.

Pondrelli, S., Morelli, A., Ekström, G., Mazza, S., Boschi, E. & Dziewonski, A. M., 2002. European-Mediterranean regional Centroid Moment Tensors Catalog: 1997–2000, *Phys. Earth Planet. Int.*, **130**, 71–101.

Pondrelli, S., Morelli, A. & Ekström, G., 2004a. European-Mediterranean regional Centroid Moment Tensor Catalog: solutions for the years 2001 and 2002, *Phys. Earth Planet. Int.*, **145**(1/4), 127–147.

Pondrelli, S., Piromallo, C. & Serpelloni, E., 2004b. Convergence vs. Retreat in Southern Tyrrhenian Sea: insights from kinematics, *Geophys. Res. Lett.*, **31**, L0661, doi:10.1029/2003GL019223.

Ray, J., Dong, D. & Altamimi, Z., 2004. IGS reference frames: status and future improvements, paper presented at IGS 2004 Workshop, Berne, Switzerland, 1 March.

Rebai, S., Philip, H. & Taboada, A., 1992. Modern tectonic stress field in the mediterranean region: evidence For variation in stress directions at different scale, *Geophys. J. Int.*, **110**, 106–140.

Rossi, S. & Sartori, R., 1981. A seismic reflection study of the external Calabrian Arc in the N Ionian Sea (Eastern Mediterranean), *Mar. Geophys. Res.*, **4**, 403–426.

Roure, F., Howell, D. G., Mueller C. & Moretti, I., 1990. Late Cenozoic subduction complex of Sicily, *J. Struct. Geol.*, **22**, 259–266.

Scandone, P. *et al.,* 1981. Mesozoic and cenozoic rocks from the Malta Escarpment (central Mediterranean), *Am. Assoc. Petr. Geol. B.*, **65**, 1299–1319.

Searle, R., 1980. Tectonic pattern of the Azores spreading centre and triple junction, *Earth Planet. Sci. Lett.*, **51**, 415–345.

Seber, D., Barazangi, M., Ibenbrahim, A. & Demnati, A., 1996. Geophysical evidence for lithospheric delamination beneath the Alboran Sea and Rif-Betic mountains, *Nature*, **379**, 785–790.

Sella, G. F., Dixon, T. H. & Mao, A., 2002. REVEL: a model for Recent plate velocities from space geodesy, *J. Geophys. Res.*, **107**(B4), doi:10.1029/2000JB000033.

Selvaggi, G. & Chiarabba, C., 1995. Seismicity and P-wave velocity image of the southern Tyrrhenian subduction zone, *Geophys. J. Int*, **121**, 818–826.

Serpelloni, E., Anzidei, M., Baldi, P., Casula, G., Galvani, A., Pesci, A,. & Riguzzi, F., 2002. Combination of permanent and non-permanent GPS networks for the evaluation of the strani-rate field in the central Mediterranean area, *Boll. Geofis. Teor. Appl.*, **43**, 195–219.

Serpelloni, E., Anzidei, M., Baldi, P., Casula, G. & Galvani, A., 2005. Crustal velocity and strain-rate fields in Italy and surrounding regions: new results from the analysis of permanent and non-permanent GPS networks, *Geophy. J. Int.*, **161**(3), 861–880. doi:10.1111/j.1365–246X.2005.02618.x.

Snoke, A. W., Schamel, S. & Karasek, R., 1988. Structural evolution of Djebel Debadib anticline: a clue to regional tectonic style of the Tunisian Atlas, *Tectonics*, **7**, 497–516.

Stampfli, G., Marcoux, J. & Baud, A., 1991. Tethyan margins in space and time, *Palaeogeogr. Palaeocl.*, **87**, 373–410.

Stampfli, G., Mosar, J., Favre, P., Pillevuit, A. & Vannay, J.C., 2001. Permo-Mesozoic evolution of the western Tethyan realm: the Neotethys-East Mediterranean basin connection, in *Peri-Tethyan Rift/Wrench Basins and Passive Margins*, Mem. Mus. d'Histoire Nat., Vol.186, pp. 51–108, eds Ziegler, P., Cavazza, W., Robertson, A.H.F.R.. & Crasquin-Soleau, S, Editions du Muséum, Paris.

Torné, M., Fernàndez, M., Comas, M. C. & Soto, J. I., 2000. Lithospheric structure beneath the alboran basin: results from 3D gravity modeling and tectonic relevance, *J. Geophys. Res.*, **105**, 3209–3228.

Tortorici, L., Monaco, C., Tansi, C. & Cocina, O., 1995. Recent and active tectonics in the Calabrian arc (Southern Italy), *Tectonophysics*, **243**, 37–55.

Turner, S. P., Platt, J. P., George, R. M., Kelley, S. P.. Pearson D. G. & Nowell, G. M., 1999. Magmatism associated with orogenic collapse of the Betic-Alboran Domain, SE Spain, *J. Petrol.*, **40**, 1011–1036.

Valensise, G. & Pantosti, D., 2001a. The investigation of potential earthquake sources in peninsular Italy: a review, *J. Seism.*, **5**, 287–306.

Van Der Meer, F. & Cloetingh, S., 1993. Intraplate stresses and subsidence history of the Sirte Basin (Libya), *Tectonophysics*, **226**, 37–58.

Vannucci, G. & Gasperini, P., 2003. A database of revised fault plane solutions for Italy and surrounding regions, *Comput. Geosci.*, **29**, 903–909.

Vannucci, G. & Gasperini, P., 2004. The new release of the database of Earthquake Mechanisms of the Mediterranean Area (EMMA Version 2), *Ann. Geophys.*, **47**(Suppl 1), 307–334.

Vannucci, G., Pondrelli, S., Argnani, A., Morelli, A., Gasperini, P. & Boschi, E., 2004. An Atlas of Mediterranean seismicity, *Ann. Geophys.*, **47**(Suppl 1), 247–306.

Vially, R., Letouzey, J., Bernard, F., Haddadi, N., Desforges, G., Askri, H. & Boudjema, A., 1994. Basin inversion along the North African Margin. The Saharan Atlas (Algeria), in *Peri-Tethyan Platforms*, pp. 9–118, 79—118, ed. Roure, F.., Technip, Paris.

Watts, A. B., Platt, J. P. & Buhl, P., 1993. Tectonic evolution of the Alboran Sea Basin, *Besin Res.*, **5**, 153–177.

Wdowinski S. *et al.,* 2004. GPS measurements of current crustal movements along the Dead Sea Fault, *J. Geophys. Res.*, **109**, B05 403, doi:10.1029/2003JB002640.

Wessel, P. & Smith, W. H. F., 1995. New version of the generic mapping tools released, *EOS Trans.*, **76**, 329.

Westaway R., 1990. Present-day kinematics of the plate boundary zone between Africa and Europe, from the Azores to the Aegean, *Earth Plan. Sci. Lett.*, **96**, 393–406.

Westaway, R., 1992. Seismic moment summation for historical earthquakes in Italy: tectonic implications, *J. Geophys. Res.*, **97**, 15 437–15 464.

Westaway, R., 1993. Quaternary uplift of southern Italy, *J. Geophys. Res.*, **97**, 15 437–15 464.

Wildi, W., 1983. La chaine tello-rifaine (Algerie, Maroc, Tunisia): structure, stratigraphie et evolution du Trias au Miocene, *Rev. Geol. Dyn. Geogr. Phys.*, **24**, 201–297.

Wortel, M. J. R. & Spakman, W., 2000. Subduction and slab detachment in the Mediterranean-Carpathian region, *Science*, **290**, 1920–1917.

Zitellini, N., Rovere, M., Terrinha, P., Chierici, F., Matias, L. & BIGSET TEAM, 2004. Neogene through Quaternary tectonic reactivation of SW Iberian passive margin, *Pure Appl. Geophys.*, **161**, 565–587.